LANGMUIR

pubs.acs.org/Langmuir Article

Mechanisms of Air Entraining of Proteins in Cementitious Materials

Mohammad Sadegh Tale Masoule, Elvis Baffoe, and Ali Ghahremaninezhad*

Cite This: https://doi.org/10.1021/acs.langmuir.4c00762 Read Online

ACCESS | Metrics & More | Article Recommendations

ABSTRACT: While few prior studies examined the air-entraining properties of proteins in cementitious materials, the underlying mechanisms of proteins' air entraining and the interactions between proteins and cement have not been studied in the past. The significance of this article is to address this knowledge gap by investigating the effect of proteins on relevant factors that affect air entraining in cement paste and establishing an understanding of the mechanism of air entrainment with proteins. These factors include the surface tension of pore solution, protein adsorption on cement particles, cement paste hydrophobization, and flow of fresh paste. Thirteen different proteins were used to investigate the effect of a wide range of protein characteristics on air entraining. Proteins decreased the pore solution surface tension to different degrees. At low concentrations, the adsorption of proteins on cement particles slightly affected the pore solution surface tension. Protein adsorption on cement particles showed a wide range of adsorption isotherms. Proteins generally increased the flow of paste due to electrostatic repulsion between cement particles because of the adsorption of negatively charged proteins on cement particles, as well as the ball-bearing effect of bubbles in fresh paste. The surface hydrophobicity was increased in pastes with proteins. A detailed microcomputed tomography (micro-CT) analysis showed very different air void microstructures in pastes with various proteins. While a relatively strong correlation was observed between air void porosity and surface hydrophobicity, the correlation between air void porosity and the surface tension of pore solution was weak. This indicates that the accumulation of hydrophobized cement particles on the air bubble in the fresh paste, refered to as the Pickering effect, is the main mechanism of air entraining of proteins in the paste. It was shown that a high air void porosity occurs in an intermediate range of flow.

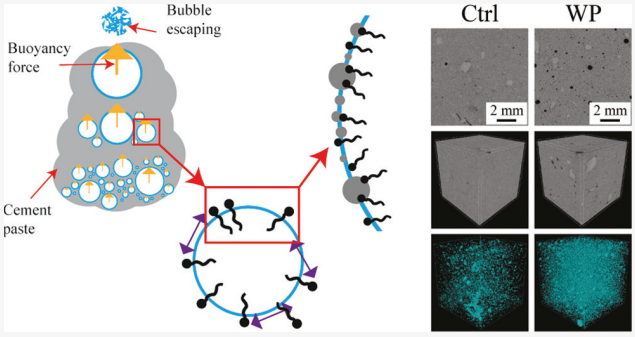

1. INTRODUCTION

1.1. Overview. Air entrainment is the process of incorporating fine air bubbles inside a cementitious mixture by adding chemical admixtures called air-entraining agents (AEA)[1] and is one of the methods of improving concrete's resistance to freeze−thaw.[2] AEA increases the initial volume of bubbles formed, bubble longevity, and resistance to different destabilizing forces.[3,4] Air entraining improves the resistance of concrete structures to freeze−thaw action. According to the hydraulic pressure theory, when the water in the capillary pores freezes during the freeze−thaw process, it expands by around 9% in volume and can exert hydraulic pressure on the microstructure, which crushes the matrix incrementally during repeated cycles.[1] Other notable theories, including osmotic pressure, critical saturation, crystallization pressure, and microlens theories, have also been proposed to model the damage sustained during freeze−thaw cycles.[5] Adjacent air-entrained voids can lessen the pressure of trapped water and ice in the capillary pores and reduce the damage to the microstructure, as well as reduce the overall degree of saturation of the concrete.[1,6−8] While the porosity of entrained air voids is important, parameters including void size distribution and spacing are also very influential on the freeze−thaw performance.[1] Entrained air voids are usually between 0.01 to 1 mm in size and primarily near-spherical. In contrast, the entrapped air voids—the air that is included in the concrete without using admixtures—are larger in size, usually higher than 1 mm, and take less spherical shapes.[1,9] In the microstructure, large voids are on average farther from each other and so have less interconnectivity,[10] which is why smaller well-dispersed voids show better freeze−thaw resistance compared to the larger voids for the same total air-entrained porosity.[10]

Surfactants can adsorb on the air−water interfaces and improve the conditions for bubble formation and stability by lowering the surface tension.[10−12] The molecular structure of surfactants generally consists of a nonpolar hydrophobic tail

Received: March 1, 2024
Revised: April 26, 2024
Accepted: June 4, 2024

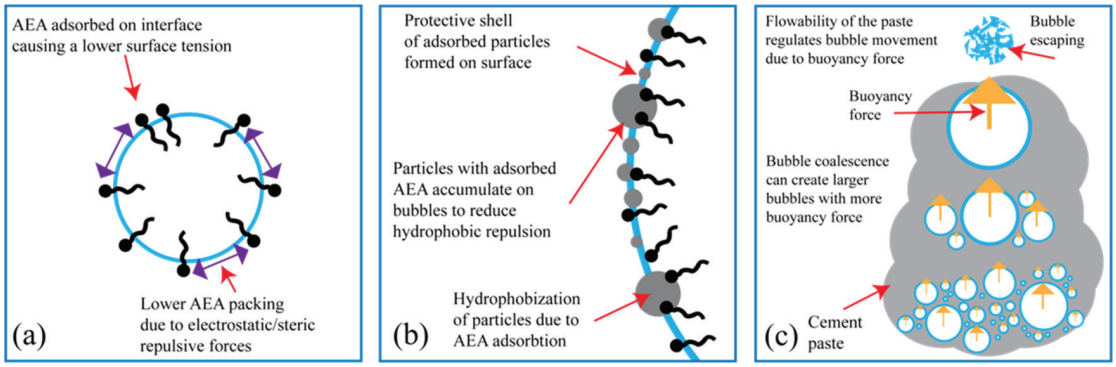

Figure 1. Summary of the interactions in cement paste between air-entraining agents, bubbles, and cement particles. (a) Adsorption on the air/water interface and the reduction of surface tension, (b) the Pickering effect of particles with adsorbed AEA and the accumulation of particles on bubbles, and (c) the regulation of bubble movement and amount in cement paste through flow. Objects are not to scale.

and a polar hydrophilic, ionic head, which facilitates surfactants' adsorption on different substrates.[10,13] Many proteins extracted from animal and plant sources, including albumin from eggs, keratin from bovine hair and hooves, collagen from bone glue or hide, and glutens found in wheat and casein milk products, can also act as surface active agents due to the presence of hydrophobic segments in their molecular structure.[14−16] Proteins have been used throughout history as an additive in construction materials,[16−18] and more recently, studies were performed on the use of protein foaming agents in cementitious environments,[15,19−25] such as those found in milk,[26−31] blood,[32−38] or plants.[39−41] It was found that proteins can undergo conformational changes, including denaturation of the secondary and tertiary structures, hydrolysis, and salt formation when exposed to cement pore solution.[15,28] One study found that proteins can create smaller voids than synthetic admixtures,[42] although their microstructure varies significantly based on their type and concentration.[43]

1.2. Mechanisms of Air Entrainment in Cement Paste by AEA. Generally, the mechanism of the AEA is the reduction of the surface tension of the pore solution by adsorbing on the air−water interface of the bubbles and stabilizing the foam through a decreased Laplace pressure.[7,10,44,45] The effect of AEA adsorption on the bubble interface and the reduction of surface tension is shown in Figure 1a. The lower Laplace pressure aids in mitigating destabilizing interactions in foams such as gas diffusion, coalescence, and drainage.[7,10,44,45] This is important since the amount of foam an AEA generates and the foam stability directly influence the total air content of hardened concrete.[7,10,45]

When foam is incorporated into the cement mixture, the system becomes much more complex, as many other interactions are involved. The adsorption of AEA on the cement particles hydrophobizes the particle surface. This adsorption promotes the accumulation of hydrophobized particles on the bubble interface—referred to as the Pickering stabilization of the particles—which forms a protective shell around the bubble and can increase bubble stability.[46−48] Figure 1b depicts these adsorbed particles and the protective interfacial film that they create. The properties of these interfacial films, such as packing density of AEA and particles, viscoelastic properties, and thickness, are very complex and can significantly influence their stability and subsequently the air content of hardened concrete.[44] Although the surface tension reduction of pore solution is an essential driver of foam formation, in some cases, the surface tension was not reduced noticeably, but high air entraining was observed.[7] On the other hand, cement pastes with similar surface tension of the pore solution can have vastly different air-entrained density and capillary microstructures.[12] This observation emphasizes the importance of other factors, including the accumulation of solid particles on the bubble film and enhancing the stability of the foam.[7,46,49]

The adsorption of AEA is influenced by their electrostatic charge, steric size, and hydrophobic interactions, among others.[7,10,45,50,51] The adsorption of AEA on cement particles makes the particles hydrophobic. Hence, the particles tend to adsorb on air−water interfaces to reduce the hydrophobic repulsive forces and, in doing so, form a protective shell around bubbles.[7,50,51] While a certain degree of hydrophobicity can improve particle adsorption on the bubble interface and foaming stability, very hydrophobic particles might not be able to pack well enough on the interface or might make the bubbles too hydrophobic and insoluble.[7] Higher ionic charge is not always beneficial either and can adversely affect the stability of bubbles in some cases, as more ionic repulsion in the interface leads to a lower AEA packing density on the air−water interface and lower foam stability.[7] Figure 1a shows the influence of the packing density of AEA in the air−water interface on the forces they exert on each other. Since cement pore solution contains ions, including Na^+, K^+, and Ca^{2+}, their interactions with anionic AEA can lead to insoluble products that alter the efficiency of AEA in the mixture. This interaction can be adverse by reducing the concentration of the AEA in the solution, or can be positive by adsorbing on the bubble and contributing to the film stability.[7,46,50] However, the extent of this interaction still needs to be fully understood.

Other properties of fresh paste, including flow, carbon content, and interactions with other admixtures, can also affect the air entraining in the concrete mixture.[7,10,50] Flow, as depicted in Figure 1c, can regulate the movement of bubbles in the fresh paste and affect the porosity. The buoyancy forces that arise from the internal pressure of bubbles move them upward to escape from the paste. While a very flowable paste provides no inhibition against this movement, a low flowable paste can resist this force and maintain the smaller bubbles inside the paste.[10]

Utilizing animal and agricultural waste byproducts in the form of proteins and biomolecules is a much-needed step toward green chemical production, sustainable construction,

https://doi.org/10.1021/acs.langmuir.4c00762
Langmuir XXXX, XXX, XXX−XXX

and circular economy. However, the physiochemical interactions between proteins and cementitious paste are not well understood in the literature. In a very recent work by our group,[52] the physiochemical properties of proteins in cement pore solution with high pH and ionic strength were systematically investigated, and changes in proteins' characteristics compared to that in their native state were discussed. While a few prior studies investigated the foaming and air entrainment of proteins in cementitious materials,[15,19,22] the mechanisms of action of proteins were not studied and are currently not understood. The novelty of this paper is to understand the underlying mechanisms governing air entrainment in hardened cementitious materials with proteins as air-entraining agents. In addition, for the first time, a wide range of proteins with different molecular structures have been systematically studied to establish the relationship between protein physicochemical properties and cement void microstructures. More specifically, this paper investigates the effect of proteins on relevant factors, including (i) surface tension of pore solution, (ii) protein adsorption on cement particles and particle hydrophobization, and (iii) flow of the cement paste. A comprehensive void microstructure analysis was performed using X-ray microcomputed tomography (micro-CT). The dependence of air entraining on different factors is discussed in detail to provide a mechanistic understanding of the interplay among these factors.

2. MATERIALS AND METHODS

2.1. Materials and Sample Preparation. Ordinary Portland cement obtained from CEMEX was used in this study, with the oxide composition presented in Table 1. The complete list of 13 proteins and their abbreviations used as air-entraining admixtures are presented in Table 2. More information about the molecular structure and physicochemical characteristics of these proteins is provided in a prior study.[52] Cement paste mixtures containing protein and the control mixture are denoted by a C-prefix. For example, C-SC refers to the cement paste sample containing the SC protein.

Table 1. Oxide Composition of the Cement Used in the Study

composition	(%)
SiO_2	20.6
Al_2O_3	4.8
Fe_2O_3	3.5
CaO	64
MgO	0.9
Na_2O	0.1
K_2O	0.3
SO_3	3.4
LOI	2.4

Table 2. List of Abbreviated Terms Used for Proteins and Solutions in the Study

name	abbreviation	name	abbreviation
sodium caseinate	SC	non-fat milk powder	NFMP
collagen peptide	CP	soy protein isolate	SPI
whey protein	WP	mild silver protein	MSP
sodium immunoglobulin	Ig	trypsin	Try
lysozyme	Lys	pepsin	Pep
hemoglobin	Hem	bovine gelatin	BG
egg white ovalbumin	Alb	deionized water	DI
synthetic pore solution	SPS	filtrate pore solution	FPS
control sample	Ctrl		

The mixtures were prepared with a water-to-cement ratio (W/C) of 0.4 and protein concentrations of 0.25, 0.5, and 1% (w/w) of the cement. The batches were mixed with a hand-held mixer for 30 s, scraped for 10 s, mixed again for 40 s, and then poured into prism molds of dimensions 2.54 × 2.54 cm^2 and length of 25.4 cm (1 × 1 × 10 $in.^3$). The mold vibrated on a mechanical shaker for 30 s. The mixtures were cured for up to 28 days in sealed plastic wraps at a temperature of 23 °C. Micro-CT and contact angle measurements were performed on 7-day and 28-day samples, respectively.

Filtrate pore solution (FPS) was prepared by mixing cement and DI with the same procedure described above but with a W/C of 1. The paste was funneled into 50 mL graded tubes and left to rest for 30 min, after which they were double centrifuged for 5 min at 4400 rpm, and the separated solution was collected and immediately sealed in a polypropylene tube to prevent exposure to air and carbonation. The pH of FPS was measured to be around 12.6−12.9 immediately after extraction.

2.2. Methods. *2.2.1. Microcomputed Tomography (micro-CT).* X-ray microcomputed tomography is an accurate and nondestructive method of analyzing concrete microstructure and phases.[53,54] Micro-CT captures two-dimensional (2D) X-ray projections of a sample at small incremental angles using a rotating stage, which are then mathematically reconstructed to produce a three-dimensional (3D) matrix of the specimen's internal phases and shape. Because of the difference in X-ray absorption between the macro phases of a concrete sample, micro-CT can accurately map the location and shape of each macro air void, aggregate and other components, including fibers.[54] Micro-CT was performed on the 7-day hardened cement sample using a Bruker Skyscan 1273 instrument, and the reconstruction and analysis were done using NRecon and CTAn software packages, respectively. Some of the scanning and analysis settings are summarized in Table 3, which include the X-ray voltage and amperage, the X-ray filter, and the threshold value used to detect voids. Voids in the range of 10−1000 μm have been analyzed as air-entrained voids.

Table 3. Micro-CT Scan Groups of Cement Paste Specimen

filter	voltage (kV)/ amperage (μA)	exposure time (ms)	dynamic range	grayscale void threshold
Cu 0.3 mm	110/300	2100	0−0.020	80
Cu 0.5 mm	120/300	2435	0−0.025	90

The process of scanning is as follows: 15 mm core cube pastes were used for the scanning to achieve a fine resolution of 8 μm per pixel. Pastes were scanned 15 times at each 0.4° increment and averaged to obtain the shadow projection at each particular angle. For a better quality scan, pastes were categorized into two groups and analyzed with slightly different properties, which are reported in Table 3. After the scanning was finished, the images were imported into NRecon software and reconstructed into a 3D model of the microstructure. Undesirable scan artifacts, such as beam hardening and ring artifacts, were also minimized by tuning the scan settings. To perform the analysis, the 3D model was imported into CTAn software. Then, the cross-sectional images were binarized into black and white regions with a single value on the grayscale axis, termed the grayscale threshold. Pixels in the images higher than this threshold became black pixels, denoting the cement matrix, and values smaller than the threshold became white pixels, denoting air voids. The single value for the threshold was selected by comparing the different sections of various pastes and is reported for both categories in Table 3. Finally, a 3D object analysis was performed to find the different properties of voids and to build the 3D model of the voids. Microstructure parameters, including air-entrained porosity, void size, and void separation, were obtained from this analysis.

https://doi.org/10.1021/acs.langmuir.4c00762
Langmuir XXXX, XXX, XXX−XXX

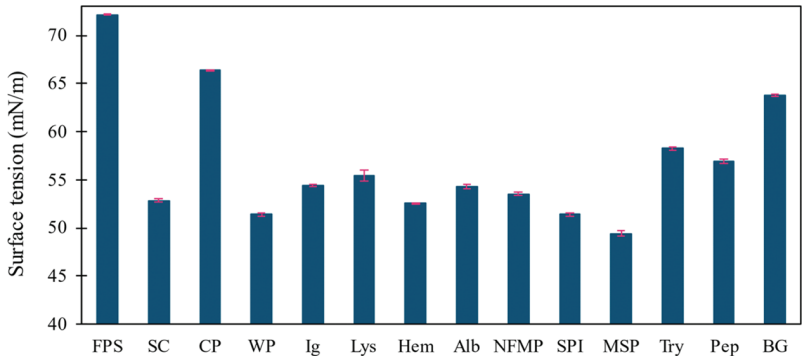

Figure 2. Surface tension of 0.5% protein concentration dissolved in FPS, extracted from fresh paste.

2.2.2. Protein Adsorption and Quantification. Protein adsorption isotherms were measured using the method described in ref 38. Cement and DI were mixed in a tube and left to rest for 20 min, after which the prepared protein solution at the measured concentration was added. The tube was ultrasonicated for 25 min and centrifuged for 10 min to separate the solution and solid phases. The supernatant was then transferred to a smaller Eppendorf tube, mixed with a BCA Protein Assay kit from Thermo Fisher, and incubated at 37 °C for 30 min. After incubation, the peak colorimetric absorbance of proteins was measured using an Agilent 8453 UV−vis spectrophotometer at 562 nm at 25 °C. The absorbance values were then converted to the adsorption of proteins on cement particles using calibration curves of each protein.

To obtain the calibration curves for each protein, six solutions of proteins in DI with different concentrations were made. Note that these solutions did not contain any cementitious materials. Then, the solutions were treated using the aforementioned procedure with the BCA Assay kit. After incubation, UV−vis was performed on these solutions, and the peak absorbance at 562 nm was measured. Plotting concentration versus this acquired peak value gives the calibration curves for one protein. This process was repeated for all proteins to obtain a calibration curve for all of them, which was then used for adsorption studies.

2.2.3. Surface Tension Measurement. The surface tension of the proteins in cement pore solutions was measured with a BZY 201 tensiometer using the platinum plate method. Solutions were allowed to rest for a few minutes to reach a stable state before the surface tension value was recorded. The measurements were repeated three to five times.

2.2.4. Flow Measurement. The flow test was performed with a modified mini cone setup according to ASTM C 1437-20, using a hollow metallic truncated cone (height: 50 mm; bottom diameter: 100 mm; top diameter: 70 mm). The cone was placed on a plate with the larger side down, and the mixture was poured in two layers. The mold was tapped 20 times with a plastic tamper. After the removal of the mold, the plate was lifted and dropped 25 times from a height of about 5 cm. The perpendicular diameters of expanded fresh cement paste were measured, and the average of three repetitions was reported as the flow of the paste. Flow tests of these pastes were performed at a W/C of 0.3.

2.2.5. Surface Hydrophobicity and Surface Profilometry. The 28-day samples were oven-dried for 24 h and then cut to expose their inner surfaces, which were used for contact angle measurements. Samples were dry-polished with silicon carbide sandpapers with grits of 180, 320, 600, and 1200. Water droplets with a volume of 2.5 μL were deposited on the cement paste surfaces, and the droplet geometries were recorded and analyzed with a high-precision camera in Biolin Scientific Attension Theta Flex. The static advancing contact angle on the cement paste surface was calculated by fitting the Young−Laplace equation to the water droplet profile. Theoretical contact angles are supposed to be descriptive of materials with homogeneous chemical characteristics and ideally smooth solid surfaces. In addition to surface chemical properties, surface physical properties, such as surface roughness, affect contact angle measurements.[55] The increase in surface roughness increases the actual contact area between the droplet and the surface compared to the projected nominal contact area. Due to the inherent porous nature of cement paste and the presence of voids of various sizes (capillary and air voids), the surface of cementitious materials has a roughness regardless of the polishing procedure used during surface preparation. Thus, it was essential that the contact angle measurements be corrected to account for the surface profile.

Surface profilometry of the polished cement surfaces was performed with a Nanovea noncontact optical profilometer using a 3500 μm chromatic confocal pen. Areas of 10 × 10 mm^2 were scanned with 5 μm increments and averaged five times per signal. The scans were then processed and analyzed using the Gwyddion 2.63 analysis tool to obtain statistics of the surface. To correct for the effect of roughness on the contact angle, Wenzel's equation[56] was used

$$\cos \theta_r = r \cos \theta_c \quad (1)$$

where θ_r is the contact angle measured on the nominal surface, θ_c is the corrected contact angle for a smooth surface—also referred to as intrinsic or Young's contact angle—and r is the roughness factor, which is the ratio of the actual surface to the projected surface. For an ideally smooth surface, r is 1, and as the roughness increases, r increases accordingly.

3. RESULTS AND DISCUSSION

3.1. Effect of Cementitious Environment on the Surface Tension of Proteins. Pore solution surface tension is an important parameter affecting air entrainment in cement mixtures and has been studied extensively for conventional surfactants.[7,44,57] AEA adsorb on the air−water interface of bubbles and considerably reduce surface tension, lowering the destabilizing Laplace pressure in the bubble.[7] Subsequently, these stable bubbles form voids in the paste and increase the porosity in the hardened cement paste. The role of surface tension in bubble formation and its stability in solution in the presence of proteins was discussed extensively in a previous work.[52] Here, the focus is mainly on protein behavior in a cementitious environment, and the reader is referred to the above-mentioned paper for further discussions related to foaming in solution media.

Figure 2 displays the surface tension of the 0.5% concentration of proteins in the extracted cement pore solution. Most proteins reduced the surface tension of FPS from around 72 mN/m (surface tension of water) to a range of 50−55 mN/m, which is a low to moderate change compared to most surfactants. Notably, some, including CP and BG, reduced surface tension insignificantly to around 65 mN/m. In a cementitious mixture, a portion of the proteins could adsorb on cement particles and be subsequently removed from the

https://doi.org/10.1021/acs.langmuir.4c00762
Langmuir XXXX, XXX, XXX−XXX

pore solution. To study how protein adsorption and reduction of free protein concentration in the pore solution influences surface tension, the surface tension of three proteins was measured in two solutions, namely, the FPS supernatant and the FPS mixture. The FPS supernatant is the case in which pore solution is extracted first and then proteins are added, whereas the FPS mixture is the case in which proteins are added during mixing and then pore solution is extracted. The results are shown in Figure 3a–c.

In most measurements, proteins have lower surface tension in the FPS supernatant compared with the FPS mixture. The main difference between the two FPS solutions is the adsorption of proteins on the cement particles. Proteins have high anionic charges in alkaline solutions and, consequently, are inclined to adsorb on the positively charged surfaces present during early hydration. Thus, the concentration of free proteins in the FPS mixture is lower, and as a result, their effect on reducing surface tension is lowered. Whereas in the FPS supernatant, proteins are added after the FPS extraction, where protein adsorption on cement does not take place. Despite this, in higher concentrations of proteins, the difference in surface tension between the two FPS solutions seems to be small, and the effect of adsorption on surface tension becomes insignificant. In high concentrations, surface tension is not affected as much because the amount of proteins in the pore solution is high, and reduction in concentration due to adsorption will not alter the surface tension that has already reached a plateau with respect to concentration.[44,57,58] It should be noted that some proteins, due to their negative surface charge, can form insoluble Ca^{2+}–protein complexes, which reduce the amount of free proteins in the solution. Such complexation could occur in both the FPS mixture and the FPS supernatant.

3.2. Adsorption of Proteins on Cement Particles.

Figure 4 displays the adsorption isotherms of proteins on cement particles in a concentration range of 200–3000 μg/mL. The variety in the isotherm shapes of proteins shows that proteins possess very different propensity for adsorption on the cement substrate. Overall, three major patterns of protein adsorption on the cement surface can be seen, including linear high adsorption,[59] a Langmuir-shaped isotherm[59] with low adsorption saturation plateau, and an isotherm in between—corresponding to MSP and SPI. At 3000 μg/mL protein content, the adsorbed protein amount on cement can range from 20% for CP and Lys and up to 100% for WP and NFMP. CP and Lys also possess relatively lower negative surface charges than other proteins at a pH of 12.6,[52] which can be one of the factors affecting their low adsorption since electrostatic force is an important mode of interaction in proteins.[60]

The adsorption behavior of proteins in high-pH solutions should be examined in two parts. The first part is the unfolding of secondary and tertiary structures[61] and disaggregation[30,62] under the effect of high pH of pore solution. The unfolding of the protein molecular structure slightly increases hydrodynamic size since the protein secondary structure occupies more space.[61] Disaggregation is generally associated with the proteins' isoelectric point (pI). Proteins at pH near their pI have negligible electrostatic repulsion, and the attractive forces—hydrophobic attractions, hydrogen bonding, and van der Waals forces[62]—can cause aggregation between them. Whereas at a pH far from protein pI, as in the case of high alkaline solutions, protein charge increases and strong

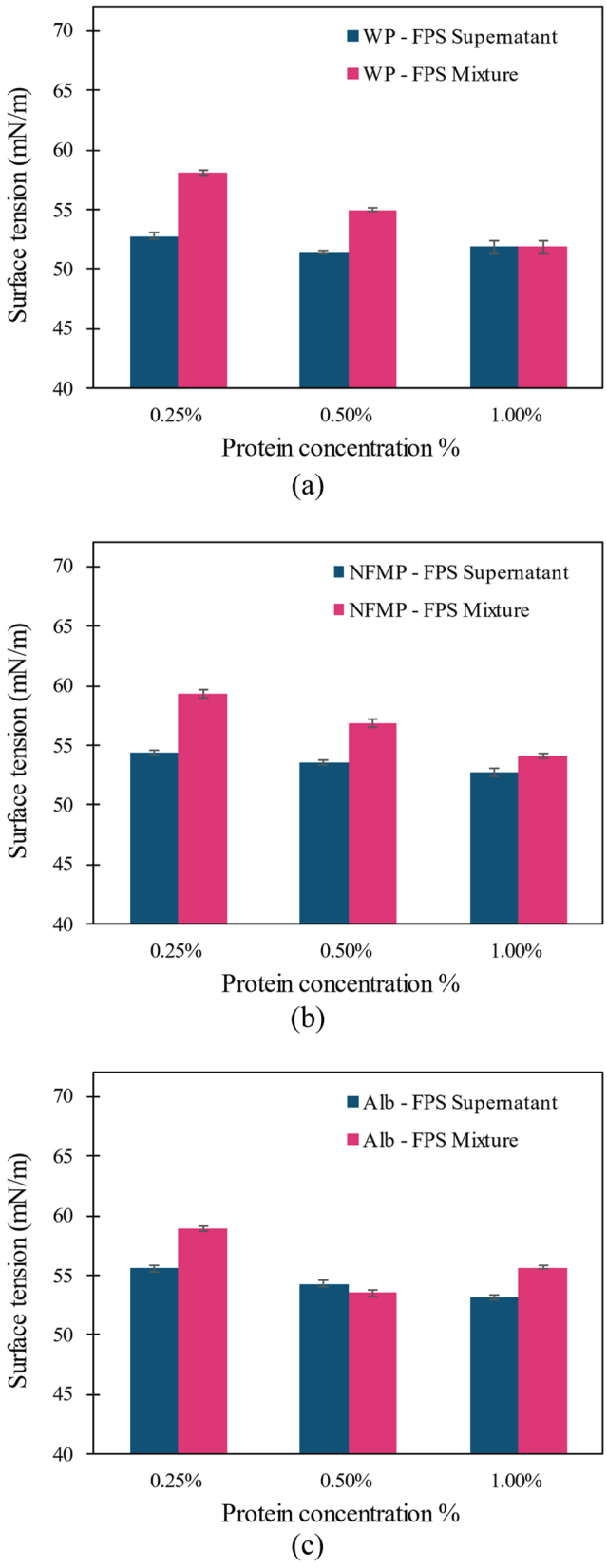

Figure 3. Surface tension of (a) WP, (b) NFMP, and (c) Alb in solutions of the FPS supernatant (the proteins were added to the extracted pore solution of cement paste) and FPS mixture (proteins were added into the cement paste mixture and then the pore solution was extracted).

https://doi.org/10.1021/acs.langmuir.4c00762
Langmuir XXXX, XXX, XXX–XXX

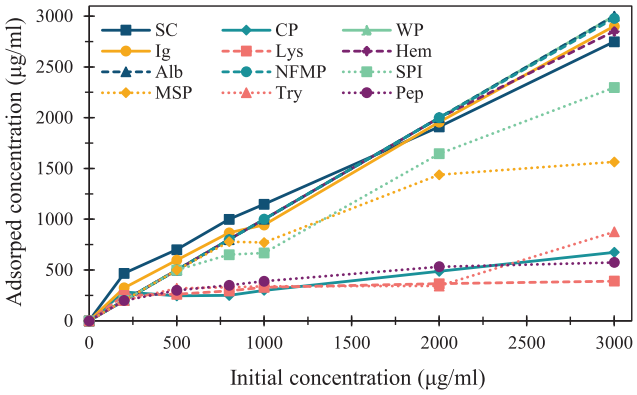

Figure 4. Adsorption isotherms of proteins on cement particles at a concentration range from 200 to 3000 μg/mL.

electrostatic repulsive forces dissociate the aggregates and result in a smaller hydrodynamic size.[62,63] The hydrodynamic size can be affected by the Ca^{2+} content as well.[64,65] Between these two mechanisms, disaggregation is usually more pronounced and reduces the hydrodynamic size of proteins.[52,62,63]

The second part is the adsorption of these negatively charged proteins on cement particles.[30] While studies on the adsorption of different biomolecules on cement are available in the literature,[66−69] proteins have received less attention.[38] Adsorption on cement particles and hydration products is governed by electrostatic interactions, hydrogen bonding, and hydrophobic attraction on unhydrated phases.[38,59,70] The partial unfolding of proteins at a high pH of cement pore solution leads to the exposure of the previously buried amino acids,[71] which entails the uncovering of charged amino acids, increasing the protein negative ζ potential,[38] polar amino acids resulting in H-bond forming forces,[70] and nonpolar amino acids resulting in modified hydrophobicity of protein solutes.[65,70,72,73] The electrostatic interactions facilitate protein adsorption on the positively charged surfaces of cement and hydration products[74] in the pore solution, as evidenced in the case of anionic surfactants.[51,75] But unlike anionic surfactants, proteins do not have hydrophobic hydrocarbon tails on one side of their structure. Instead, the hydrophobic amino acids are situated on different patches of their tertiary structure,[76] which makes the hydrophobicity dependent upon the folding state of the protein.[76] The effect of pH on the hydrophobicity of proteins seems to be very dependent on the protein itself,[77] its ζ potential interactions,[73] and the employed method of measuring hydrophobicity,[78] so much that it can show contradictory relationships with pH.[78] While in some studies, hydrophobicity of proteins increased at higher pH,[72] in other studies, it decreased in highly negatively charged environments.[73] Dispersed ionic content of the pore solution may lead to some degree of charge shielding, as it has been shown that higher Ca^{2+} of the solution can cause a decline in ζ potential and an increase in hydrodynamic size.[65] But Ca^{2+} also affects the adsorption amount through calcium bridging, in which Ca^{2+} forms complexes with negatively charged ions, including SO_4^{2-}, and amino acids and cement particle surfaces.[70,79]

Although adsorption mechanisms are important in cementitious systems, they do not seem to be the only factor affecting the microstructure of hardened paste, as proteins with similar adsorption in Figure 4, including SC and WP, have very different void structures, as will be discussed in Section 3.4. Another property of anionic surfactants is hydrophobization of the matrix because they possess a highly anionic head that can adsorb on the particle surface and form a layer of hydrophobic chains, turning the cement particle more hydrophobic in turn.[51,75] These hydrophobic particles can then adsorb on air bubbles and stabilize them in the paste, leading to higher porosity.[75]

3.3. Flow of Fresh Cement Paste. The effect of the protein concentration on the flowability of fresh cement paste is shown in Figure 5. The flow of cement paste is important in paste's ability to stabilize and maintain bubbles and can subsequently affect the air-entrained void structure of the hardened sample.[10,80] A wide range of flow values are seen across different proteins and concentrations, stipulating that physiochemical and structural differences in proteins strongly affect their ability to modify the paste characteristics. As discussed previously, high adsorption of proteins on cement can have a detrimental effect on the air entraining of proteins by reducing the available concentration of proteins at the air−water interface.[10] On the other hand, adsorbed proteins on particles can affect the flow and hydrophobicity of particle and bubble stability in cement paste.[10,80] As such, protein adsorption on cement has an indirect influence on the air-entraining performance.

In anionic superplasticizers, the negative charge facilitates the adsorption on the positively charged cementitious surfaces.[81] Adsorbed layers of superplasticizers induce repulsion between particles through elevated electrostatic and steric repulsive forces, increasing flow.[45,81,82] Steric forces

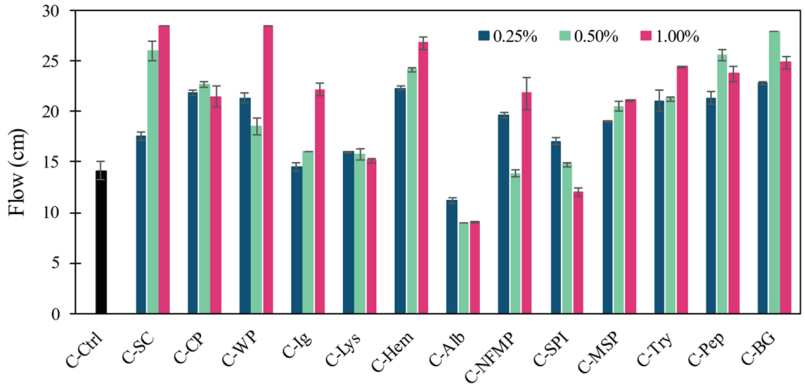

Figure 5. Flow of the cement paste specimen with various proteins at three concentrations of 0.25, 0.5, and 1% (W/C 0.3).

https://doi.org/10.1021/acs.langmuir.4c00762
Langmuir XXXX, XXX, XXX−XXX

depend on the thickness of the adsorbed protein layer on the particles, as they act through the physical inhibition of large molecules.[45] Since steric forces depend on the size of proteins, disaggregation and unfolding can affect them to some degree. As some protein aggregates can have large hydrodynamic sizes,[52] this effect can impact cement paste flow.[45]

As Figure 5 shows, some proteins, including Hem, WP, and NFMP, increase the flow significantly even at the lowest concentration, which is due to the high protein adsorption on particles and high protein negative charge creating large electrostatic repulsion between cement particles.[52] The proteins mentioned above display high adsorption on particles, as is displayed in the adsorption isotherms in Figure 4. Another contributing factor to the increased flow is the ball-bearing effect of fine bubbles smaller than 450 μm.[83] It is postulated that a high number of these fine bubbles can act as a cushion between particles and aggregates to reduce the internal friction of the paste or concrete and increase the flow of the system.[83,84] As will be discussed in the next section, proteins result in many very fine bubbles that can lead to ball-bearing interactions. Although this phenomenon is more significant in mortar and concrete where aggregates with irregular shapes and pointy corners are present,[85] it still affects the flow of cement particles in the paste. Therefore, proteins that do not adsorb much but show significant flow, including Try, Pep, and CP, are probably acting through the ball-bearing effect.

The lowest flow was observed for C-Alb, with a flow of 10 cm, which is even smaller than that of C-Ctrl, which was about 14 cm. Since the initial diameter of the flow cone is 10 cm, C-Alb has very insignificant flow, and even the change in concentration, up to 4 times higher, did not increase the flowability of the paste. Although C-Alb shows high adsorption on cement particles and a high negative charge at high alkaline pH, it has a relatively small hydrodynamic size.[52] This reduced steric repulsion might account for some of the low flow. The more probable explanation for this effect is the possible bridging action of the Alb protein and its gel formation. Ionic patches on Alb can adsorb on different adjacent particles, bind them together, and increase the mixture's internal friction, resulting in a lower flow than C-Ctrl.[31] Especially for Alb, high interfacial strength and adhesive behavior were observed in higher concentrations that can be attributed to the gel formation of the protein.[31] This adhesiveness depends on many factors, such as the adsorptive substrate properties, the denaturation state of proteins, and the protein extraction procedure.[31,86] C-SPI also decreases in flow at higher concentrations, which can be due to a combination of gel formation behavior and protein aggregation. SPI aggregates noticeably in DI, making it hard to perform some of the experiments in neutral pH. The high alkaline environment of cement pore solution significantly helps in increasing the solubility and stability of SPI and other proteins, even at lower concentrations.[52] However, some amount of aggregation of SPI can still be seen even at high pH, possibly lowering the available proteins in the bulk solution by reduced dispersibility and thus decreasing its impact on flow.

3.4. Micro-CT Characterization of the Void Structure.

3.4.1. Change in the Microstructure by the Protein Type and Concentration. The air-entraining ability of proteins is shown in Figure 6a, where air void porosity has increased as much as 18% for C-MSP compared to 0.5% for C-Ctrl. Figure 6a also shows that increasing the concentration of proteins in the cement mixture results in a higher incorporation of air into a

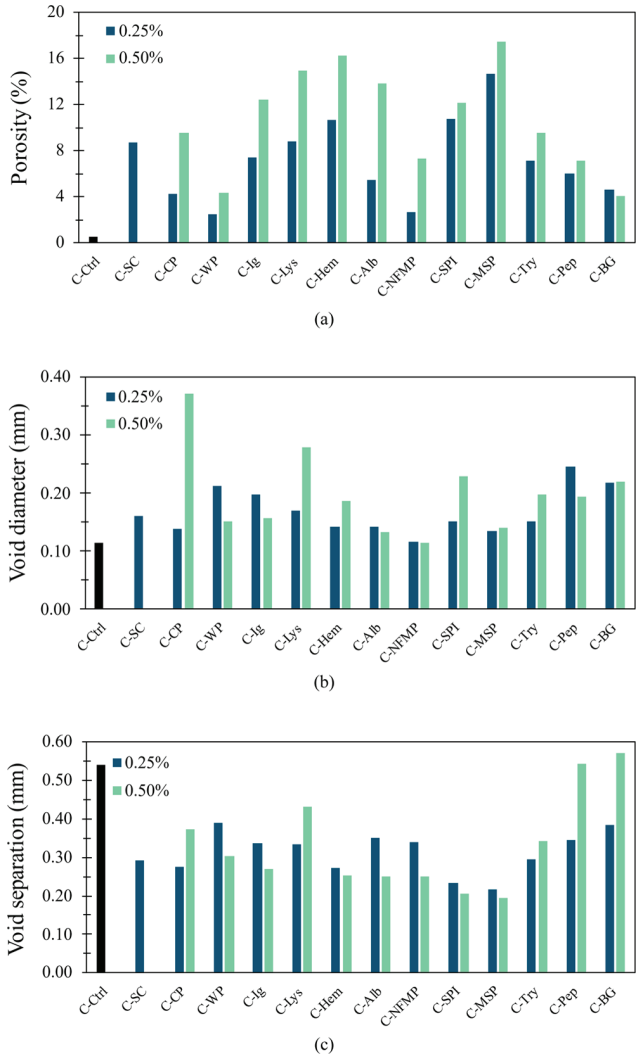

Figure 6. Effect of protein type and concentration on the air-entrained void structure of cement paste. (a) Porosity, (b) void size, and (c) separation.

hardened paste in most cases. While this change is not significant in the case of some proteins, in the case of some other proteins, including Alb, this increase is very noticeable. As discussed earlier, the effect of concentration on porosity involves interactions among a series of factors, including the physiochemical properties of the proteins,[52] the adsorption capacity of cement particles,[75] and the change in the flow of the paste.[10]

C-SC is significantly different from all of the other samples since SC suddenly changes from a potent air-entraining agent in 0.25% to an air-detraining agent in 0.5% concentration. The main reason for this is the significant increase in the flow of the mixture from 0.25 to 0.5%, as shown in Figure 5. During casting and vibration, C-SC displayed extreme bubble escape through the top surface of the cement paste. This highly fluid paste could no longer resist the bubble buoyancy forces, which led to their escape. After the hardening of C-SC, a thin layer of hardened and brittle cancellous material consisting of foams with adsorbed cement was observed on top of the sample, leaving a very dense hardened matrix with fewer voids and lower porosity than even the C-Ctrl in the bottom portion of the sample (see Figure 7a). This phenomenon is discussed in

https://doi.org/10.1021/acs.langmuir.4c00762
Langmuir XXXX, XXX, XXX−XXX

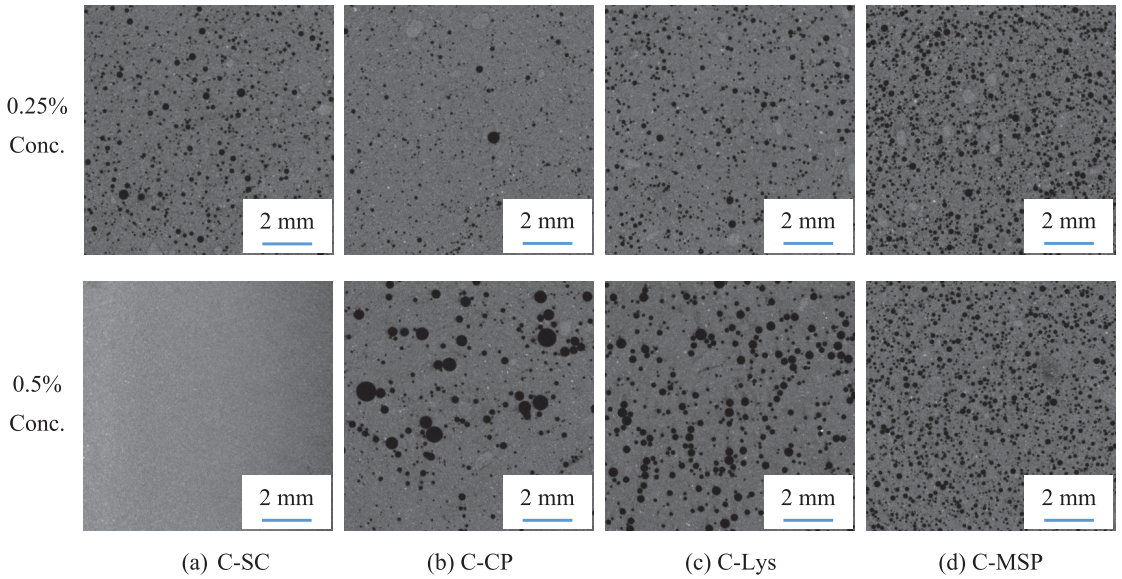

Figure 7. Micro-CT images of select samples with 0.25 and 0.5% protein concentrations.

Section 1.2 and depicted in Figure 1c, where underlying factors affecting the porosity, including the flow and buoyancy forces, were reviewed.

Figure 6b,c shows the size and separation of voids in the hardened cement paste modified with proteins. To study the distribution of air-entrained voids in the microstructure, the separation parameter has been used, which is different from the commonly used spacing factor. The spacing factor is a theoretical distance hypothesized initially by Powers based on Darcy's Law[87] to estimate the hydraulic pressure exerted on the microstructure of concrete.[88] Although useful in practice, this estimate is not a true descriptor of the 3D microstructure of air-entrained concrete, especially since more accurate parameters are available. The separation parameter used in this study is the mean thickness of the cement matrix between adjacent voids. This parameter is directly calculated from the 3D microstructure of samples scanned with micro-CT, using a sphere-fitting algorithm to determine a histogram of thickness and the mean value of separation.[89]

Despite the significant increase in air-entrained porosity in the samples with 0.5% protein compared to that with 0.25% protein, the change in the void diameter is relatively small. This is because the volume of voids is proportional to the cube of void size, and as such, small changes in size can be much more prominent on the total volume of the voids. The type of protein also affected the separation through the change in void diameter and the total number of voids. Void separation is one of the most important factors determining the air-entraining performance in freeze−thaw cycles. The smaller separation between voids leads to higher diffusion of hydraulic pressure inside the voids.[90] For example, C-Pep and C-BG do not experience a significant change in porosity between the two concentrations, but the separation increases significantly. The reason for this difference in C-Pep and C-BG lies in the shape of the void size distributions of the two concentrations. These samples have equal porosity and average void size at 0.25 and 0.5% concentrations, but different void size distributions result in different separations. This becomes more apparent when the presence of many tiny voids is considered. While these tiny voids do not affect the void volume or volume-weighted average size noticeably, they can significantly affect the average separation between voids. The reconstructed cross sections of select cement pastes with proteins are shown for the 0.25 and 0.5% concentrations in Figure 7. These images demonstrate the distinct effect of the protein type and concentration on the void structure of the cement pastes. While almost all samples experienced increased porosity with an increase in concentration, C-SC is the only exception, where it loses its bubble stability at higher protein concentrations due to a significant increase in flow, as discussed previously. Figure 7b,c shows a considerable increase in the void size and porosity in the case of C-CP and C-Lys, respectively. However, in Figure 7d, which corresponds to C-MSP, the size and porosity change were insignificant between the two concentrations.

3.4.2. Distribution of Entrained Air Voids. Volume-based void distributions are analyzed in this study. Number-based distributions are sharply skewed toward smaller sizes due to the large number of very fine voids (smaller than 50 μm) in the system. Apart from their contribution to porosity, the high quantity of very fine voids is also important in enhancing the workability of fresh paste and air network in the hardened paste.[91−93] Although some conclusions can be drawn from the number-based distribution,[91] volume-based distributions provide better insight into the effect of proteins on the void structure of cement. A significant variation in the void structure was observed between the cement pastes entrained with different protein types, as represented in Figure 7. Figure 8a displays the difference in the 3D void structure between the sample without proteins and the highly porous structure of C-MSP, and Figure 8b displays a thresholding example.

Figure 9 shows the volume fraction distribution of voids in C-Ctrl paste and pastes with four select proteins at a concentration of 0.25% and their corresponding porosity. Since only a few voids larger than 0.3 mm exist, the void distributions are plotted in the size range of 0−0.3 mm. This can be seen from the void size distribution of C-MSP plotted for a larger size range of 0−1 mm shown in the inset.

From the distributions in Figure 9, it is evident that the inclusion of proteins populated the sample with larger air-entrained voids compared to C-Ctrl. While almost 90% of

https://doi.org/10.1021/acs.langmuir.4c00762
Langmuir XXXX, XXX, XXX−XXX

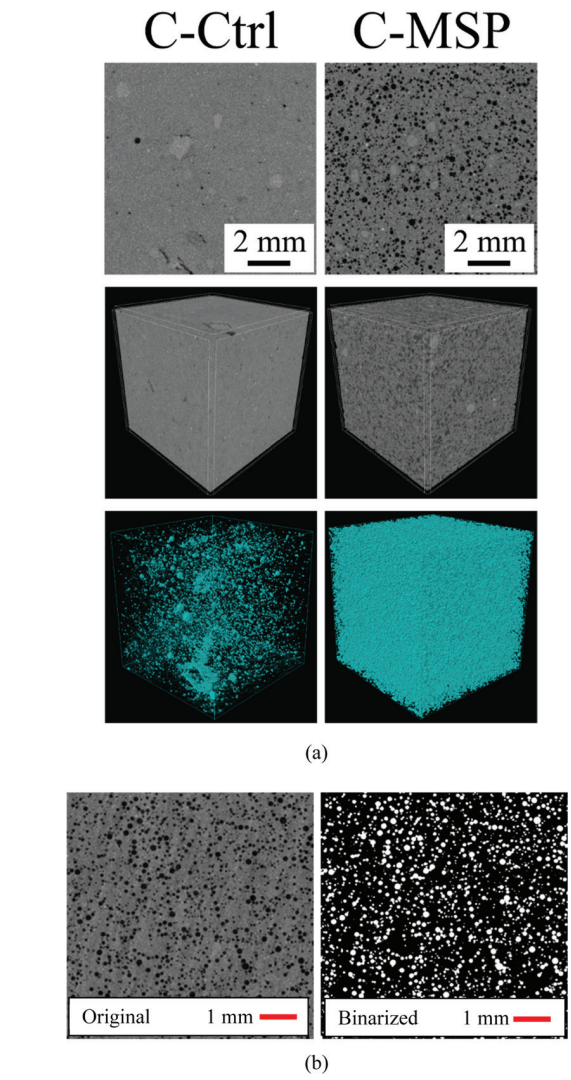

Figure 8. Micro-CT representation of C-Ctrl and C-MSP in a protein concentration of 0.25%. (a) From top to bottom, the images show (top row) the cross section of the specimen at the midpoint, (middle row) a reconstructed 3D representation of the specimen, and (bottom row) the extracted voids in the 3D model. (b) The original and binarized cross section of C-Hem 0.5% after thresholding.

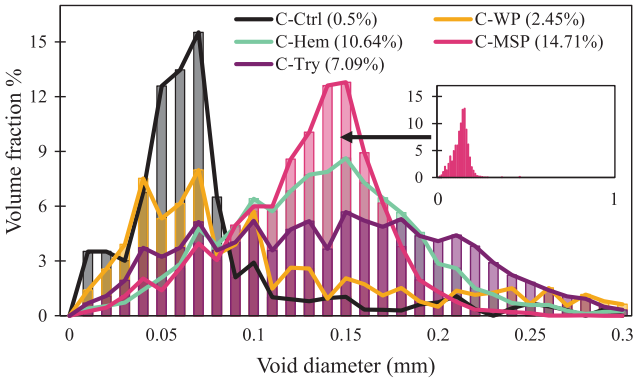

Figure 9. Volume-based distributions of the void diameter for select samples with 0.25% protein concentration. The numbers in the parentheses indicate the porosity of the specimen at this concentration.

voids in the C-Ctrl are situated at the lower bound of the void size below 0.1 mm, in protein air-entrained samples, this number shifts significantly, and the majority of voids are in the 0.1−0.2 mm range. The protein addition increased the average void diameter, shifting it from 0.11 mm for C-Ctrl to a range of 0.14−0.25 mm for samples with different proteins. Samples with protein showed a wide variety of size distributions; while sharp peaks were observed for some, including C-MSP with a peak around 0.15 mm, others showed a broader distribution in the case of C-Try. This emphasizes that the size distribution of voids is very dependent on the protein's physiochemical properties.

The C-Ctrl sample has the highest percentage of small air voids in the sub-100 μm group, and the addition of proteins lowers this skewness and shifts the air voids toward larger sizes. It is important to note that this is because proteins increase the stability of bubbles in the fresh cement paste and make it possible for bubbles of different sizes to exist in the paste, ultimately turning them into voids when the paste sets.[10] This means that in C-Ctrl, most bubbles larger than 0.1 mm coalesce together into bubbles larger than 1 mm and escape the paste, whereas, in samples with proteins, the higher stability maintains bubbles in different sizes. It is important to note the difference between C-Ctrl and samples with proteins. The voids in C-Ctrl are entrapped air pockets that are incorporated during the physical process of mixing and are not a product of a stable bubble in the paste. That is why they can quickly coalesce to form very large voids that escape during vibration due to a higher buoyancy force, leaving a lower number of finer voids. However, proteins alter the chemical interactions and create air-entrained voids through a stable bubble with a viscous film interface that can resist many destabilizing interactions in foams.

Small and well-dispersed bubbles are preferred in fresh cement paste to improve the freeze-thaw resistance. However, due to different destabilizing phenomena, including gas diffusion, bubble coalescence, and drainage,[10] bubbles become larger and escape the fresh paste aided by the buoyancy force.[10,94] Proteins can affect the rate of this expansion with varying effectiveness. For example, C-CP and C-NFMP have their voids mostly in the sub-100 μm group, while C-SC and C-Ig are moderately dispersed and have greater volumes in the 100−250 μm range, and C-Pep and C-BG are mostly populated with voids larger than 250 μm. It is important to note that void diameter is not the only factor in judging the effectiveness of proteins as air-entraining admixtures, and other factors such as porosity and separation of voids should also be considered.[1] C-Pep and C-BG, for instance, reside in the average porosity zone despite being comprised of larger voids and having higher separation compared to most protein samples, which is not generally favorable for freeze−thaw resistance.[1]

3.5. Contact Angle on Cement Paste Surface. Contact angle measurement is a quantitative method of determining the wettability of surfaces and, therefore, can reveal the hydrophobization of cement paste by proteins. Angles between water droplets and cement surface smaller than 90° indicate a hydrophilic surface, and similarly, angles larger than 90° indicate a hydrophobic surface.[55] As contact angles increase from an ideally hydrophilic surface with a contact angle of 0°, the matrix loses some of its hydrophilicity and becomes more hydrophobic.

https://doi.org/10.1021/acs.langmuir.4c00762
Langmuir XXXX, XXX, XXX−XXX

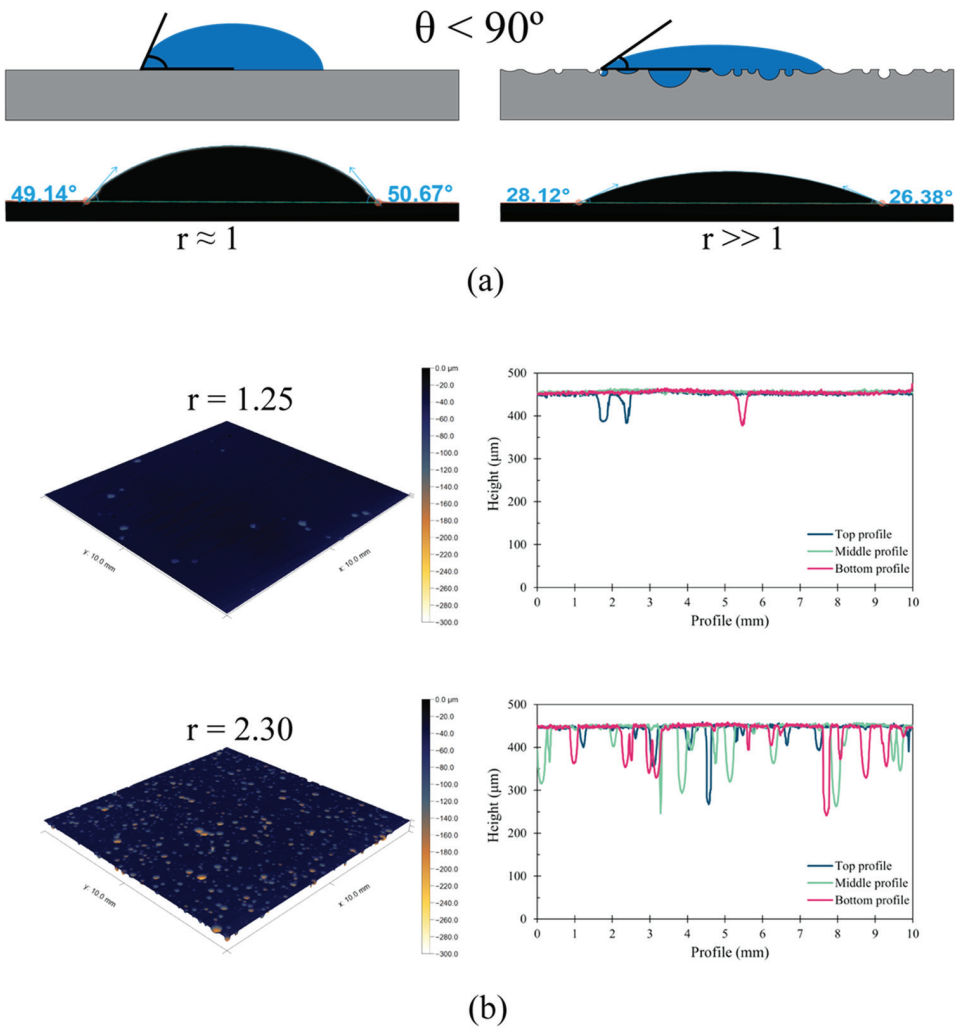

Figure 10. (a) Effect of surface roughness on the measured contact angle of the surface and (b) roughness surface and profiles of C-Ctrl (top) and C-Hem-0.5% (bottom) and the calculated *r* factors for each.

Apart from the effect of material surface chemistry on contact angle measurements, the surface's physical properties, such as surface roughness, influence contact angle measurements.[55] As indicated previously, the inherent porous nature of cementitious materials having capillary voids and air voids introduces surface roughness.[49] Figure 10a shows the effect of surface roughness on hydrophilic surfaces ($\theta < 90°$), which makes the measured angle appear smaller than the intrinsic angle on an ideally smooth surface. Since the purpose of these measurements is to determine the chemical properties of the cement matrix and not their topological effects on the contact angles, the corrected contact angles are calculated and reported. The corrections are made by scanning the surface of the sample with a noncontact profilometer and calculating the *r* factor, which is the ratio of the developed surface to the projected surface, shown in Figure 10b. Then, using Wenzel's relation (eq 1), corrected contact angles are calculated. Table 4 displays the profilometry results and the ratios measured for different samples at both 0.25 and 0.5% concentrations. Wenzel's model assumes that surface asperities are much smaller than the droplet volume,[95] which is valid for the majority of samples in this study.

The measured contact angle is dependent on the method and type of cement hydrophobization.[55] External surface

Table 4. Results of Profilometry Analysis on Polished Cement Paste Specimen with 0.25 and 0.5% Protein Concentration of Cement[a]

	0.25%			0.5%		
specimen	Sa (μm)	Sz (μm)	Wenzel *r*	Sa (μm)	Sz (μm)	Wenzel *r*
Ctrl	3.9	154.9	1.252	3.9	154.9	1.252
SC	8.7	348.7	1.638	2.4	31.7	1.253
CP	3.4	227.5	1.368	31.3	836.9	1.744
WP	4.1	294.0	1.255	5.5	375.6	1.319
Ig	6.9	272.7	1.433	13.5	715.7	1.884
Lys	10.6	276.2	1.769	32.1	1044.0	2.286
Hem	12.0	348.2	1.873	23.8	514.7	2.297
Alb	4.1	192.8	1.324	9.6	415.3	1.582
NFMP	3.3	151.9	1.251	5.8	327.2	1.446
SPI	13.1	352.6	1.865	10.0	279.9	1.738
MSP	19.3	356.9	2.322	13.3	341.4	1.826
Try	6.3	220.3	1.427	12.3	391.5	1.715
Pep	5.8	210.4	1.343	13.7	409.4	1.669
BG	5.2	178.6	1.279	9.0	280.4	1.501

[a]Sa and Sz are the arithmetic mean height and maximum height according to ISO 25178 and Wenzel *r* is the ratio of developed area to projected area of the surface.

https://doi.org/10.1021/acs.langmuir.4c00762
Langmuir XXXX, XXX, XXX−XXX

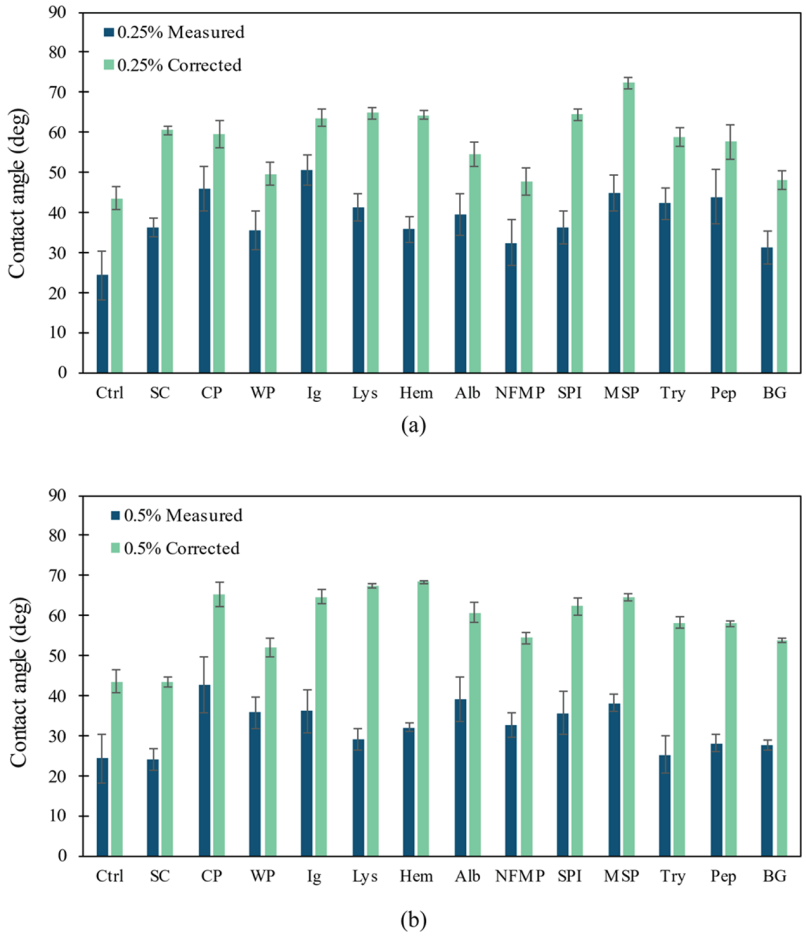

Figure 11. Contact angle measurements of 28-day cement paste specimens with different proteins at concentrations of (a) 0.25% and (b) 0.5%. Measured contact angles are obtained from the surface and corrected for topography with Wenzel's equation.

applications such as coating generally give higher contact angles compared to internal mixing of the hydrophobizing agent in concrete.[31,96] Although contact angles as high as 162° for superhydrophobic cement have been achieved,[55,97] the normal range of contact angles in the literature for internally hydrophobized cement paste is lower, and plain cement samples have an angle around 40−50°,[55,96,98,99] which is consistent with the corrected contact angle of C-Ctrl in this study. The measured contact angles, displayed in Figure 11, have a range of 20−50°, and since the *r* factor is much larger than 1 for all samples, corrected contact angles increase to a range of 40−70°. The measurements show that proteins display some degree of cement hydrophobization, but this effect is not as substantial as some synthetic hydrophobizing agents.[55]

C-Ctrl has the lowest corrected contact angle at around 43.5°, and all other samples display higher corrected contact angles due to the hydrophobic properties of added proteins. As mentioned in the previous section, C-SC experiences severe depletion of bubbles from the top surface due to the very high flowability of the fresh paste in 0.5% concentration. These bubbles carry a significant amount of protein with them to the top and lower the protein amount in the paste. Because of this effect, the corrected contact angle on C-SC drops from 60.49° at 0.25% concentration to 43.25° at 0.5% concentration, very closely matching the contact angle of C-Ctrl. For other proteins, the contact angle did not change significantly between 0.25 and 0.5%, except for a few that showed lower contact angles.

3.6. Discussions on Parameters Affecting the Air-Entraining Performance of Proteins in Cement.

3.6.1. Effect of Surface Tension and Foam Volume on Entrained Air in Hardened Paste. Figure 12a−c displays the effect of surface tension of different proteins on air void characteristics of hardened cement paste for two different concentrations of 0.25 and 0.5%. Although surface tension is usually noted as the most important factor in the air entraining of cement,[44] other factors, such as adsorption and flow, can also contribute to the air-entraining performance. It has been reported that the dosages of surfactants above the critical micelle concentration—the concentration at which surface tension plateaus—continue to increase porosity despite having constant surface tension.[57] This is apparent in Figure 12a, where the samples with 0.5% concentration show a higher porosity compared to the samples with 0.25% protein; however, the relationship between surface tension and porosity becomes weaker in higher concentrations of proteins (0.5 vs 0.25%). As shown in Figure 12a−c, a decrease in surface tension correlates with higher air-entrained porosity, smaller voids, and lower separation between voids. This behavior can be primarily attributed to a higher volume of stable foam, in which bubbles can resist disjoining and destabilizing forces without coalescing or escaping the cement mixture,[10] and subsequently a more porous hardened paste.

https://doi.org/10.1021/acs.langmuir.4c00762
Langmuir XXXX, XXX, XXX−XXX

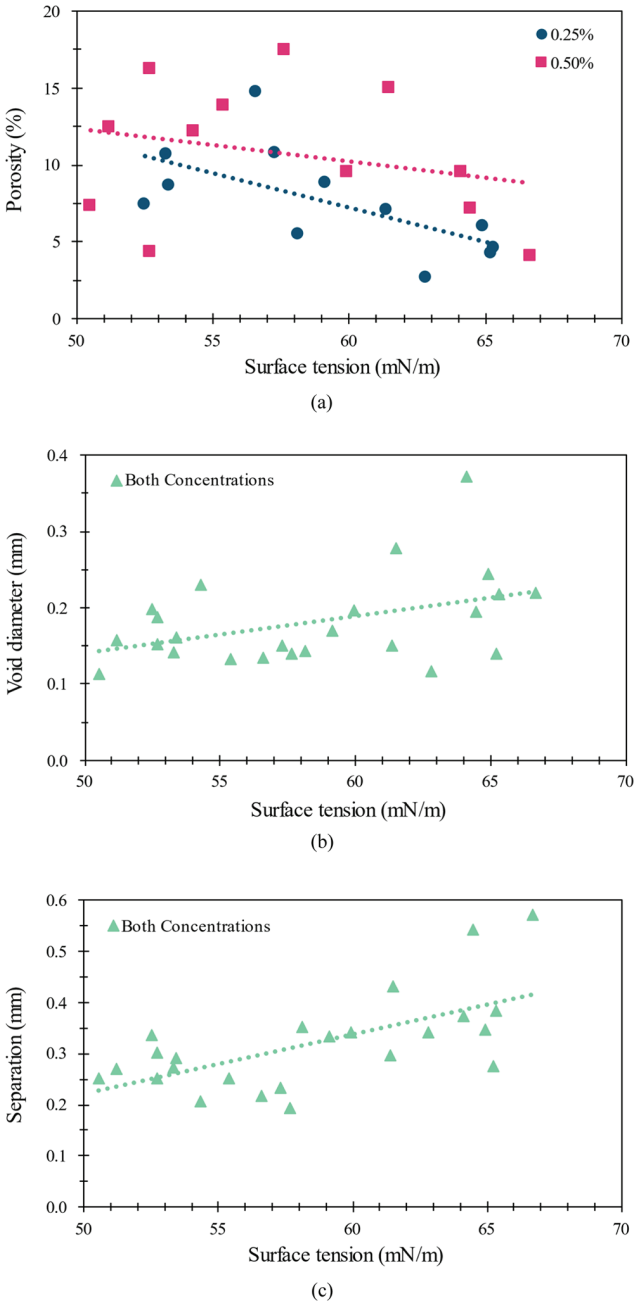

Figure 12. Relationship between surface tension and void characteristics in hardened cement paste: (a) porosity, (b) void diameter, and (c) separation.

3.6.2. Effect of Foam Volume on the Porosity of Hardened Sample. It is difficult to directly correlate the properties of the solution with the final porosity of the hardened cement paste. This is because many of the important interactions, including adsorption of proteins to particles, hydrophobization, and Pickering, occur when the cement particles are present in the mixture. Despite this, a very good correlation is observed between the foam volume in the pore solution and the air-entrained porosity of samples in this study, as depicted in Figure 13. The foam volume measurements are taken from a previous study by the same authors, where the effect of physicochemical properties of cement pore solution on the foaming behavior of proteins were explored.[52] This compelling

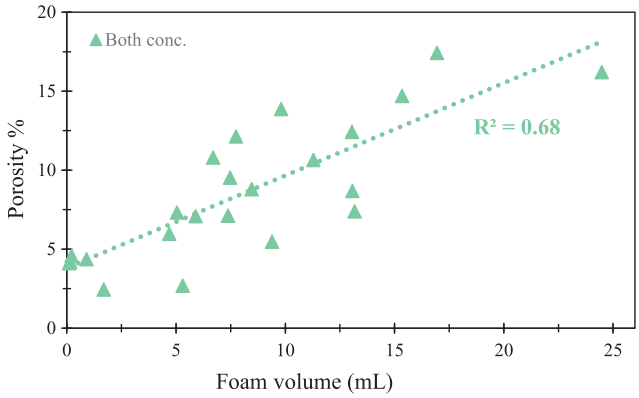

Figure 13. Impact of foam volume (both 0.25 and 0.5% concentrations) on the porosity of hardened cement paste.

connection between the foam volume of proteins and the corresponding porosity in the hardened cement paste stipulates the fact that generally, a protein capable of producing and maintaining a large amount of bubbles in the solution will also be effective in incorporating a higher porosity of air voids in cement paste.

Previous studies have shown similar trends between the foaming volume in the solution and the properties of hardened concrete.[100,101] The results show that as the volume of foam increases in the solution, the porosity of concrete increases and density and strength decline, especially for protein-based agents.[102,103] Higher volume of foam does not only mean that the protein is able to produce more bubbles but that the interface between bubbles is also stronger. This is because proteins unfold and attain a high anionic charge in the alkaline environment of the pore solution. The higher charge and modified protein structure can facilitate higher adsorption of proteins on the bubble interface and the formation of a mesh network with cations present. This gives the interface improved elasticity and viscosity and increases its stability.[52] In the cementitious mixture, the adsorption of hydrophobic particles on the interface and the formation of the protective shell further enhance the stability.

3.6.3. Effect of Fresh Paste Properties on the Porosity of Hardened Sample. As discussed before, the higher negative electrostatic charge enhances the adsorption of proteins on both air bubbles and cement particles, as observed with anionic surfactants.[30] The repulsive electrostatic force from adsorbed proteins on bubbles and hydrophobized particles can help stabilize air bubbles. Anionic bubbles can also adsorb on cement grains and form complexes. Subsequently, the sphere of negative forces around particles and bubbles acts as a lubricative agent and reduces the internal friction between the particles, which leads to higher flow.[104] This is shown in Figure 14a, which displays the influence of the protein concentration and flow on the porosity of air-entrained samples. The behavior curve of 0.5% concentration sits above that of 0.25%, showing the relatively positive effect of concentration on porosity.

Another important interpretation of the flow-porosity relationship is the dependence on the relative rate of flow. While in 0.25%, flow values above 20 cm seem too high and result in lower relative porosities, in 0.5% concentration, even flows around 20−25 cm give high porosity values. This is due to the balance of interactions and forces in the paste. While a higher concentration results in higher flow that can be

https://doi.org/10.1021/acs.langmuir.4c00762
Langmuir XXXX, XXX, XXX−XXX

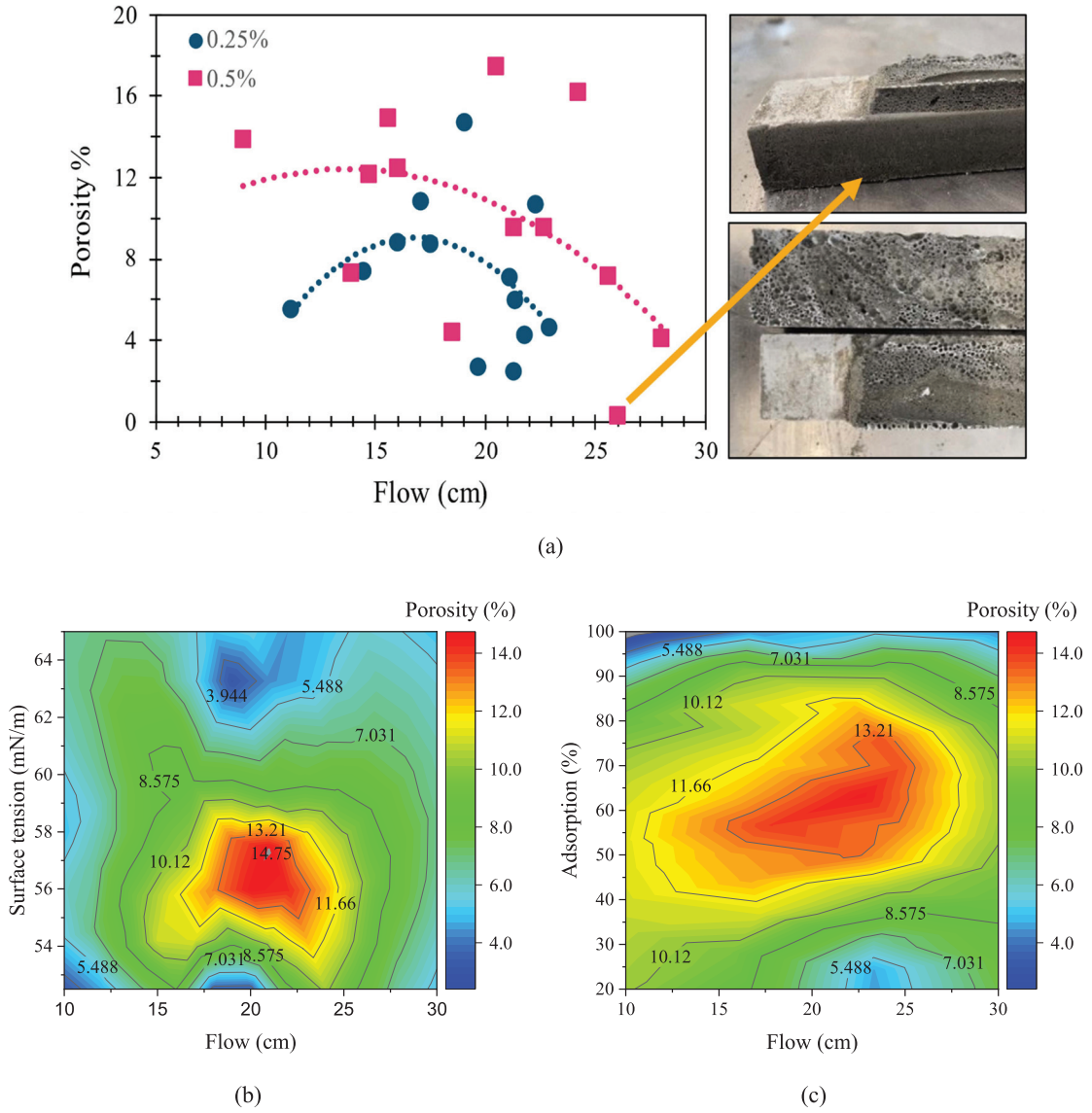

Figure 14. Relation between the flow, porosity, and physicochemical properties of the cement paste samples at concentrations of 0.25 and 0.5%. (a) Images show the detrimental effect of high flow, which caused the escape of bubbles entrained in C-SC at 0.5% concentration. (b, c) Graphs include both concentrations. Adsorption is the amount adsorbed at 3000 μg/mL. Some outliers were removed, and the contour plots were smoothened.

detrimental to porosity, it also strengthens favorable interactions such as lower surface tension and higher adsorption on the bubble interface that stabilize the mixture. It appears that extremely low or high flow of fresh paste can be detrimental and result in low air incorporation or quick decline of the entrained air, as is evident by the concave trend in Figure 14a. If the flow is too low, the incorporation of air during mixing through vortex action is low,[94] and if it is too high, bubbles can more easily coalesce and escape due to the upward buoyancy forces.[10] The highest percentages of air occur in pastes with a medium range of flow in their respective concentrations.

The low flow portion of Figure 14a is not represented very well since most proteins acted as good plasticizers, but the very highly flowable part is well characterized, especially by very fluid C-SC in 0.5% concentration. While C-SC had substantial porosity in 0.25% concentration with a medium flow of around 17.5 cm, its flow increased significantly to 26 cm in 0.5%. This highly flowable paste was unable to inhibit the buoyancy-induced movement of bubbles, and so all bubbles escaped before the paste could set. The final porosity of C-SC is even less than that of the C-Ctrl. The remaining shell of these escaped bubbles at the top of the C-SC sample can be seen in Figure 14a, where a white layer of deposited SC protein shows the border between the dense part at the bottom and the extremely cancellous foam remaining at the top. This cancellous part was so weak that the smallest force exerted by fingers broke it off into powder.

Contour plots of Figure 14b,c present the combined effects of the properties of fresh cement paste on the porosity of hardened samples. As discussed previously and observed in Figure 14b, the high porosity region marked in red is located at low surface tension and medium flow ranges. The combined effect of adsorption and flow can be seen in Figure 14c, where high porosity is reached when both the flow and adsorption of the proteins on particles are in the medium region. Medium to

https://doi.org/10.1021/acs.langmuir.4c00762
Langmuir XXXX, XXX, XXX−XXX

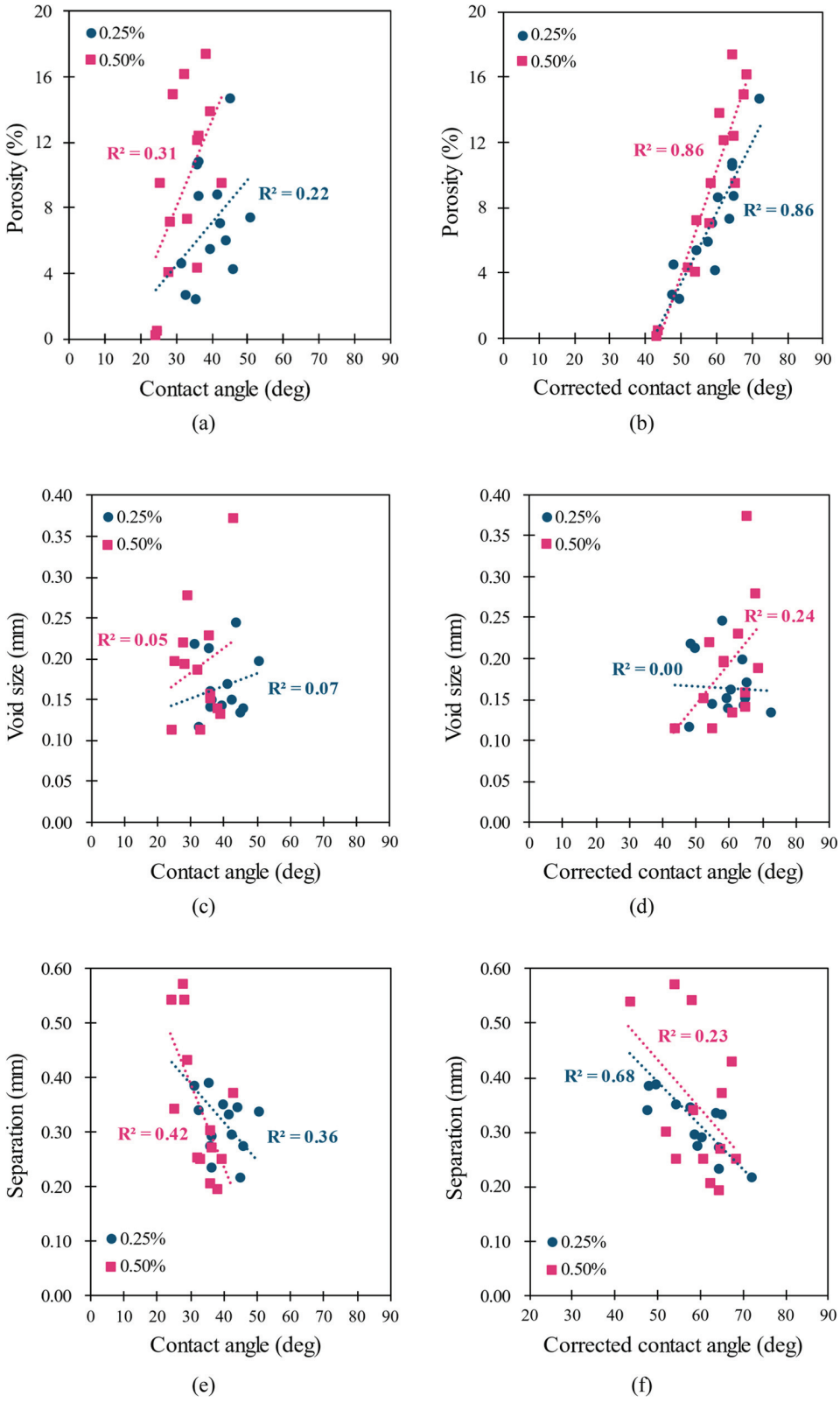

Figure 15. Relationship between the contact angle on cement paste and the air-entrained void properties. A few outliers have been removed.

low porosity correlates with very high adsorption, displaying the negative effect of high adsorption on particles in the air entraining of proteins.

3.6.4. Effect of Paste Hydrophobicity on the Air-Entrained Properties. It is informative to understand how the hydrophobization of cement particles by protein adsorption affects the air-entrained properties. Cement particle's hydrophobization changes the interface of bubbles in the fresh paste and influences the microstructure of the hardened paste. The change in bubble stability is mainly through Pickering

https://doi.org/10.1021/acs.langmuir.4c00762
Langmuir XXXX, XXX, XXX−XXX

stabilization, which is the accumulation of particles with adsorbed surfactants on the air−water interface, which can influence bubble stability.[75] In cement, the adsorption of particles on the interface creates a protective shell that improves the stability of air voids.[46,51] This is shown in Figure 1b, where it can be seen that proteins first adsorb on the particles and increase the particle's hydrophobicity. These particles then migrate to the interface of bubbles and create a protective shell that can significantly increase the stability of bubbles to destabilizing forces in the mixture.

Previous studies have discussed that one of the important properties that determines the adsorption of particles on the air−water interface of bubbles and the subsequent bubble stability is the particle's contact angle.[105,106] In bubble systems, a very high or low contact angle is not beneficial to the stability of the bubbles, and the optimum theoretical contact angle for the highest bubble stability lies below 90°, usually in the range of 60−70°.[107] This angle range minimizes the destabilizing phenomena that occur between adjacent bubbles, including thinning of the interfacial layers by raising the capillary pressure needed for coalescence.[107] Very high contact angles beyond 90° can have destabilizing effects on the bubble system.[105] It should be noted that the optimum contact angle might be different in cementitious mixtures.

Figure 15 displays the effect of cement hydrophobization and Pickering stabilization on the void properties in hardened cement paste. The results involving both measured and corrected contact angles are displayed for comparison. Figure 15a,b shows that the air-entrained porosity of the cement paste is positively dependent on the contact angle, and the highest porosity occurs at the greatest contact angles. Neither measured nor corrected contact angles show a meaningful correlation with the void size shown in Figure 15c,d. Separation, on the other hand, has an inverse correlation with the contact angle, as seen in Figure 15e,f, and the strength of the correlation does not differ between the two contact angles. Lower separation at a higher contact angle means that many of the smaller bubbles are stable in the paste and do not coalesce or diffuse, resulting in a higher number of voids with short separation between them.

As Figure 15 displays, the type of correlation does not change between measured and corrected contact angles, and only the strength of the correlations changes. The corrected contact angle has a very strong correlation with porosity, some of which might be due to biases associated with contact angle correction. This is because the r factor is a metric of the 3D surface and has a correlation with microstructure properties, especially porosity. Correcting contact angles with r and then comparing them with micro-CT results will introduce some bias into the results that need to be considered. That is why both measured and corrected contact angles are shown to account for the biases and get a more realistic picture of the influences. It is important to note that regardless of the bias, the correlation is strong between the porosity and contact angle and displays the important influence of particle hydrophobization and Pickering on bubbles.

4. CONCLUSIONS

The air-entraining mechanisms of 13 proteins with different characteristics in cementitious materials were examined in this study. The following conclusions can be drawn from the results below.

- Proteins showed a wide range of surface tension values in cement pore solution. At a low concentration, the adsorption of proteins on cement particles reduces the amount of free proteins in the pore solution, which reduces the protein effect on the surface tension of the pore solution. However, with increasing concentration, the effect of protein adsorption on cement particles did not seem to affect the surface tension of the pore solution.
- Proteins exhibited different adsorption isotherms on cement particles. While some proteins, such as Lys, showed very low adsorption and quickly reached a plateau, others showed noticeably higher adsorption. The negative charge of the proteins at a high pH of cement paste facilitates their adsorption on cement particles through electrostatic interactions.
- The proteins generally increased the flow of the cement paste. The increased electrostatic repulsion between cement particles due to the adsorption of negatively charged proteins on cement particles, as well as the ball-bearing effect of air bubbles in the fresh paste, can explain the increased flow in cement paste with proteins. Protein adsorption also increased the hydrophobicity of the hardened paste and resulted in surface contact angles as high as 70°.
- Proteins greatly affected the air-entrained void structure in hardened cement paste. Proteins increased the void porosity up to 17.4% in the paste, while void size and separation had a smaller range of changes. These results show the potential of proteins as an air-entraining admixture for cementitious materials and how the type and concentration of proteins significantly affect void structure.
- A relatively strong correlation between air void porosity and foam volume was observed, as well as between the porosity and paste contact angle. However, the correlation between porosity and surface tension was not as strong. It was shown that pastes with an intermediate range of flow exhibited a higher porosity, indicating the stabilizing effect of flow against buoyancy forces. The correlation between the contact angle and porosity points to the Pickering effect as a primary mechanism of air entraining of proteins in cement pastes.

AUTHOR INFORMATION

Corresponding Author

Ali Ghahremaninezhad − *Department of Civil and Architectural Engineering, University of Miami, Coral Gables, Florida 33146, United States;* orcid.org/0000-0001-9269-801X; Phone: (+1) 305-2843465; Email: a.ghahremani@miami.edu

Authors

Mohammad Sadegh Tale Masoule − *Department of Civil and Architectural Engineering, University of Miami, Coral Gables, Florida 33146, United States*

Elvis Baffoe − *Department of Civil and Architectural Engineering, University of Miami, Coral Gables, Florida 33146, United States*

Complete contact information is available at: https://pubs.acs.org/10.1021/acs.langmuir.4c00762

https://doi.org/10.1021/acs.langmuir.4c00762
Langmuir XXXX, XXX, XXX−XXX

Notes

The authors declare no competing financial interest.

■ ACKNOWLEDGMENTS

This study was supported in part by the National Science Foundation under the CAREER award number 1846984 and the MRI award number 1920127. Any opinions, findings, conclusions, or recommendations expressed in this material are those of the author(s) and do not necessarily reflect the views of the National Science Foundation. The authors would like to thank Drs. Amin and Knecht for allowing access to their laboratories to conduct contact angle and adsorption experiments.

■ REFERENCES

(1) Dodson, V. H. *Concrete Admixtures*; Springer US, 1990.
(2) Mousavinezhad, S.; Gonzales, G. J.; Toledo, W. K.; Garcia, J. M.; Newtson, C. M.; Allena, S. A Comprehensive Study on Non-Proprietary Ultra-High-Performance Concrete Containing Supplementary Cementitious Materials. *Materials* **2023**, *16*, No. 2622.
(3) Zeng, X.; Lan, X.; Zhu, H.; Liu, H.; Umar, H. A.; Xie, Y.; Long, G.; Ma, C. A Review on Bubble Stability in Fresh Concrete: Mechanisms and Main Factors. *Materials* **2020**, *13*, No. 1820.
(4) Petit, P.; Javierre, I.; Jézéquel, P.-H.; Biance, A.-L. Generation and stability of bubbles in a cement based slurry. *Cem. Concr. Res.* **2014**, *60*, 37−44.
(5) Guo, J.; Sun, W.; Xu, Y.; Lin, W.; Jing, W. Damage Mechanism and Modeling of Concrete in Freeze−Thaw Cycles: A Review. *Buildings* **2022**, *12*, No. 1317.
(6) Eriksson, D.; Gasch, T.; Ansell, A. A Hygro-Thermo-Mechanical Multiphase Model for Long-Term Water Absorption into Air-Entrained Concrete. *Transp. Porous Media* **2019**, *127*, 113−141.
(7) Tunstall, L. E.; Ley, M. T.; Scherer, G. W. Air entraining admixtures: Mechanisms, evaluations, and interactions. *Cem. Concr. Res.* **2021**, *150*, No. 106557.
(8) Li, W.; Pour-Ghaz, M.; Castro, J.; Weiss, J. Water Absorption and Critical Degree of Saturation Relating to Freeze-Thaw Damage in Concrete Pavement Joints. *J. Mater. Civ. Eng.* **2012**, *24*, 299−307.
(9) Neville, A. M. *Properties of Concrete: Fourth and Final Edition*; Wiley, 1997.
(10) Du, L.; Folliard, K. J. Mechanisms of air entrainment in concrete. *Cem. Concr. Res.* **2005**, *35*, 1463−1471.
(11) Ramachandran, V. S. Concrete Admixtures Handbook: Properties, Science and Technology Elsevier Science, 1996.
(12) Masoule, M. S. T.; Ghahremaninezhad, A. Effect of Poly-(ethylene glycol)−Poly(propylene glycol) Triblock Copolymers on Autogenous Shrinkage and Properties of Cement Pastes. *Buildings* **2024**, *14*, No. 283.
(13) Kashani, A.; Ngo, T. D.; Nguyen, T. N.; Hajimohammadi, A.; Sinaie, S.; Mendis, P. The effects of surfactants on properties of lightweight concrete foam. *Mag. Concr. Res.* **2020**, *72*, 163−172.
(14) Schwaminger, S.; Blank-Shim, S. A.; Borkowska-Panek, M.; Anand, P.; Fraga-García, P.; Fink, K.; Wenzel, W.; Berensmeier, S. Experimental characterization and simulation of amino acid and peptide interactions with inorganic materials. *Eng. Life Sci.* **2018**, *18*, 84−100.
(15) Chandra, S.; Aavik, J. Influence of proteins on some properties of portland cement mortar. *Int. J. Cem. Compos. Lightweight Concr.* **1987**, *9*, 91−94.
(16) Krizova, I.; Schultz, J.; Nemec, I.; Cabala, R.; Hynek, R.; Kuckova, S. Comparison of analytical tools appropriate for identification of proteinaceous additives in historical mortars. *Anal. Bioanal. Chem.* **2018**, *410*, 189−200.
(17) Hewlett, P. C.; Liska, M.*Lea's Chemistry of Cement and Concrete*; Elsevier, 2019; pp 1−858.
(18) Torgal, F. P.; Ivanov, V.; Karak, N.; Jonkers, H. *Biopolymers and Biotech Admixtures for Eco-efficient Construction Materials*; Elsevier, 2016.
(19) Jitchaiyaphum, K.; Sinsiri, T.; Chindaprasirt, P. Cellular Lightweight Concrete Containing Pozzolan Materials. *Procedia Eng.* **2011**, 1157−1164.
(20) Bing, C.; Zhen, W.; Ning, L. Experimental Research on Properties of High-Strength Foamed Concrete. *J. Mater. Civ. Eng.* **2012**, *24*, 113−118.
(21) Falliano, D.; de Domenico, D.; Ricciardi, G.; Gugliandolo, E. Mechanical Characterization of Extrudable Foamed Concrete: An Experimental Study. *Int. J. Civ. Environ. Eng.* **2018**, *12*, 228−232.
(22) Kearsley, E. P.; Wainwright, P. J. The effect of porosity on the strength of foamed concrete. *Cem. Concr. Res.* **2002**, *32*, 233−239.
(23) Vazquez, A.; Pique, T. M. Biotech Admixtures for Enhancing Portland Cement Hydration. *Biopolymers and Biotech Admixtures for Eco-Efficient Construction Materials*; Elsevier Inc., 2016; pp 81−98.
(24) Bezerra, U. T. Biopolymers with Superplasticizer Properties for Concrete. *Biopolymers and Biotech Admixtures for Eco-Efficient Construction Materials*; Elsevier Inc., 2016; pp 195−220.
(25) Plank, J. Applications of Biopolymers in Construction Engineering. *Biopolymers Online*; John Wiley & Sons, Inc., 2005.
(26) Dias de Souza, C.; Gonçalves Dias de Souza, N. L.; Gomes Barbosa, M. T.; Stephani, R.; Cappa de Oliveira, L. F. Investigation the sustainable additive influence, obtained from milk protein, in the chemical and physical properties of Portland cement. *Composites, Part B* **2019**, *175*, No. 107148.
(27) Chang, I.; Im, J.; Chung, M. K.; Cho, G. C. Bovine casein as a new soil strengthening binder from diary wastes. *Constr. Build. Mater.* **2018**, *160*, 1−9.
(28) Jagannathan, P.; Parameswaran, P. The study on the characteristics of concrete by partial replacement of cement with fly ash enriched with Casein protein. *Int. J. Civ. Eng. Technol.* **2017**, *8*, 2187−2197.
(29) Bian, H.; Plank, J. Effect of heat treatment on the dispersion performance of casein superplasticizer used in dry-mix mortar. *Cem. Concr. Res.* **2013**, *51*, 1−5.
(30) Plank, J.; Bian, H. Method to assess the quality of casein used as superplasticizer in self-levelling compounds. *Cem. Concr. Res.* **2010**, *40*, 710−715.
(31) Baffoe, E.; Ghahremaninezhad, A. On the interaction between proteins and cracked cementitious surface. *Constr. Build. Mater.* **2022**, *352*, No. 128982.
(32) Jasiczak, J.; Zielinski, K. Effect of protein additive on properties of mortar. *Cem. Concr. Compos.* **2006**, *28*, 451−457.
(33) Al-Rim, K. Etude de l'influence de différents facteurs d'allègement des matériaux argileux: Le béton argileux léger, généralisation à d'autres fines roches et applications à la conception d'éléments de construction préfabriqués, 1995.
(34) Ruzika, M. Optimisation d'un procède de moussage protéinique de pates argile-ciment: conséquences sur le comportement physicomécanique du matériau durci. Thèse de doctorat, Université de Rennes, 1998.
(35) Ruzicka, M.; t'Kint de Roodenbeke, A.; Dheilly, R. M.; Qéneudec, M. *A Lightening Process of Clay Cement Pastes by Recycled Ox-blood*; CIB World Building Congress, 1998.
(36) Chikhi, A.; Queneudec, M.; Dheilly, R. M. Reuse of food industry by-products: animal protein as a workability enhancing admixture. DOI: 10.1680/ROWM.32521.0035.
(37) Remadnia, A.; Dheilly, R. M.; Laidoudi, B.; Quéneudec, M. Use of animal proteins as foaming agent in cementitious concrete composites manufactured with recycled PET aggregates. *Constr. Build. Mater.* **2009**, *23*, 3118−3123.
(38) Baffoe, E.; Ghahremaninezhad, A. The effect of biomolecules on enzyme-induced calcium carbonate precipitation in cementitious materials. *Constr. Build. Mater.* **2022**, *345*, No. 128323.
(39) Shanmugavel, D.; Selvaraj, T.; Ramadoss, R.; Raneri, S. Interaction of a viscous biopolymer from cactus extract with cement

paste to produce sustainable concrete. *Constr. Build. Mater.* **2020**, *257*, No. 119585.
(40) Zhang, M. Y.; Zhao, H.; Zhang, Q. The production of protein foaming agent from baijiu vinasse. *Appl. Mech. Mater.* **2014**, 688−692.
(41) Chandra, S.; Eklund, L.; Villarreal, R. R. Use of cactus in mortars and concrete. *Cem. Concr. Res.* **1998**, *28*, 41−51.
(42) Panesar, D. K. Cellular concrete properties and the effect of synthetic and protein foaming agents. *Constr. Build. Mater.* **2013**, *44*, 575−584.
(43) Chandni, T. J.; Anand, K. B. Utilization of recycled waste as filler in foam concrete. *J. Build. Eng.* **2018**, *19*, 154−160.
(44) Tunstall, L. E.; Scherer, G. W.; Prud'homme, R. K. Studying AEA interaction in cement systems using tensiometry. *Cem. Concr. Res.* **2017**, *92*, 29−36.
(45) Feneuil, B.; Pitois, O.; Roussel, N. Effect of surfactants on the yield stress of cement paste. *Cem. Concr. Res.* **2017**, *100*, 32−39.
(46) Ley, M. T.; Chancey, R.; Juenger, M. C. G.; Folliard, K. J. The physical and chemical characteristics of the shell of air-entrained bubbles in cement paste. *Cem. Concr. Res.* **2009**, *39*, 417−425.
(47) Cervantes-Álvarez, A.; Escobar-Ortega, Y. Y.; Sauret, A.; Pacheco-Vázquez, F. Air entrainment and granular bubbles generated by a jet of grains entering water. *J. Colloid Interface Sci.* **2020**, *574*, 285−292.
(48) Ren, Y.; Zhu, G.; Tang, J. Synthesis of cement shell microcapsules via W/O Pickering emulsions. *Colloids Surf., A* **2020**, *584*, No. 124073.
(49) Ley, M. T.; Folliard, K. J.; Hover, K. C. Observations of air-bubbles escaped from fresh cement paste. *Cem. Concr. Res.* **2009**, *39*, 409−416.
(50) Tunstall, L. E.; Scherer, G. W.; Prud'homme, R. K. A new hypothesis for air loss in cement systems containing fly ash. *Cem. Concr. Res.* **2021**, *142*, No. 106352.
(51) Bruere, G. M. Air-entraining actions of anionic surfactants in portland cement pastes. *J. Appl. Chem. Biotechnol.* **1971**, *21*, 61−64.
(52) Masoule, M. S. T.; Baffoe, E.; Ghahremaninezhad, A. On the physicochemical properties and foaming characteristics of proteins in cement environment. *Constr. Build. Mater.* **2023**, *366*, No. 130204.
(53) Peng, Y.; Zhao, G.; Qi, Y.; Zeng, Q. In-situ assessment of the water-penetration resistance of polymer modified cement mortars by μ-XCT, SEM and EDS. *Cem. Concr. Compos.* **2020**, *114*, No. 103821.
(54) du Plessis, A.; Boshoff, W. P. A review of X-ray computed tomography of concrete and asphalt construction materials. *Constr. Build. Mater.* **2019**, *199*, 637−651.
(55) Zhao, J.; Gao, X.; Chen, S.; Lin, H.; Li, Z.; Lin, X. Hydrophobic or superhydrophobic modification of cement-based materials: A systematic review. *Composites, Part B* **2022**, *243*, No. 110104.
(56) Wenzel, R. N. Resistance of solid surfaces to wetting by water. *Ind. Eng. Chem.* **1936**, *28*, 988−994.
(57) Şahin, Y.; Akkaya, Y.; Boylu, F.; Taşdemir, M. A. Characterization of air entraining admixtures in concrete using surface tension measurements. *Cem. Concr. Compos.* **2017**, *82*, 95−104.
(58) Kitabatake, N.; Doi, E. Surface Tension and Foamability of Protein and Surfactant Solutions. *J. Food Sci.* **1988**, *53*, 1542−1569.
(59) Nguyen, D. D.; Devlin, L. P.; Koshy, P.; Sorrell, C. C. Impact of water-soluble cellulose ethers on polymer-modified mortars. *J. Mater. Sci.* **2014**, *49*, 923−951.
(60) Mahmoudi, M.; Lynch, I.; Ejtehadi, M. R.; Monopoli, M. P.; Bombelli, F. B.; Laurent, S. Protein-nanoparticle interactions: Opportunities and challenges. *Chem. Rev.* **2011**, *111*, 5610−5637.
(61) Qadeer, A.; Rabbani, G.; Zaidi, N.; Ahmad, E.; Khan, J. M.; Khan, R. H. 1-Anilino-8-Naphthalene Sulfonate (ANS) Is Not a Desirable Probe for Determining the Molten Globule State of Chymopapain. *PLoS One* **2012**, *7*, No. e50633.
(62) Lam, R. S. H.; Nickerson, M. T. The effect of pH and temperature pre-treatments on the physicochemical and emulsifying properties of whey protein isolate. *LWT—Food Sci. Technol.* **2015**, *60*, 427−434.
(63) Chen, N.; Lin, L.; Sun, W.; Zhao, M. Stable and pH-sensitive protein nanogels made by self-assembly of heat denatured soy protein. *J. Agric. Food Chem.* **2014**, *62*, 9553−9561.
(64) Subirade, M.; Chen, L.Food-Protein-Derived Materials and Their Use as Carriers and Delivery Systems for Active Food Components. *Delivery and Controlled Release of Bioactives in Foods and Nutraceuticals*; Elsevier, 2008; pp 251−278.
(65) Zhang, J.; Liang, L.; Tian, Z.; Chen, L.; Subirade, M. Preparation and in vitro evaluation of calcium-induced soy protein isolate nanoparticles and their formation mechanism study. *Food Chem.* **2012**, *133*, 390−399.
(66) Ouyang, X.; Qiu, X.; Chen, P. Physicochemical characterization of calcium lignosulfonate—A potentially useful water reducer. *Colloids Surf., A* **2006**, *282*−*283*, 489−497.
(67) Poinot, T.; Bartholin, M. C.; Govin, A.; Grosseau, P. Influence of the polysaccharide addition method on the properties of fresh mortars. *Cem. Concr. Res.* **2015**, *70*, 50−59.
(68) Bülichen, D.; Kainz, J.; Plank, J. Working mechanism of methyl hydroxyethyl cellulose (MHEC) as water retention agent. *Cem. Concr. Res.* **2012**, *42*, 953−959.
(69) Zhang, D. F.; Ju, B. Z.; Zhang, S. F.; He, L.; Yang, J. Z. The study on the dispersing mechanism of starch sulfonate as a water-reducing agent for cement. *Carbohydr. Polym.* **2007**, *70*, 363−368.
(70) Picker, A.; Nicoleau, L.; Nonat, A.; Labbez, C.; Cölfen, H. Identification of Binding Peptides on Calcium Silicate Hydrate: A Novel View on Cement Additives. *Adv. Mater.* **2014**, *26*, 1135−1140.
(71) Kamali, M.; Ghahremaninezhad, A. Effect of Biomolecules on the Nanostructure and Nanomechanical Property of Calcium-Silicate-Hydrate. *Sci. Rep.* **2018**, *8*, No. 9491.
(72) Uruakpa, F. O.; Arntfield, S. D. Surface hydrophobicity of commercial canola proteins mixed with κ-carrageenan or guar gum. *Food Chem.* **2006**, *95*, 255−263.
(73) Paulson, A. T.; Tung, M. A. Solubility, Hydrophobicity and Net Charge of Succinylated Canola Protein Isolate. *J. Food Sci.* **1987**, *52*, 1557−1561.
(74) Labbez, C.; Jönsson, B.; Pochard, I.; Nonat, A.; Cabane, B. Surface Charge Density and Electrokinetic Potential of Highly Charged Minerals: Experiments and Monte Carlo Simulations on Calcium Silicate Hydrate. *J. Phys. Chem. B* **2006**, 9219−9230.
(75) Tunstall, L. E.; Scherer, G. W.; Prud'homme, R. K. A new hypothesis for air loss in cement systems containing fly ash. *Cem. Concr. Res.* **2021**, *142*, No. 106352.
(76) van Dijk, E.; Hoogeveen, A.; Abeln, S. The Hydrophobic Temperature Dependence of Amino Acids Directly Calculated from Protein Structures. *PLoS Comput. Biol.* **2015**, *11*, No. e1004277.
(77) Ponnuswamy, P. K. Hydrophobic characteristics of folded proteins. *Prog. Biophys. Mol. Biol.* **1993**, *59*, 57−103.
(78) Alizadeh-Pasdar, N.; Li-Chan, E. C. Y. Comparison of Protein Surface Hydrophobicity Measured at Various pH Values Using Three Different Fluorescent Probes. *J. Agric. Food Chem.* **2000**, 328−334.
(79) Zingg, A.; Winnefeld, F.; Holzer, L.; Pakusch, J.; Becker, S.; Gauckler, L. Adsorption of polyelectrolytes and its influence on the rheology, zeta potential, and microstructure of various cement and hydrate phases. *J. Colloid Interface Sci.* **2008**, *323*, 301−312.
(80) Barfield, M.; Ghafoori, N. Air-entrained self-consolidating concrete: A study of admixture sources. *Constr. Build. Mater.* **2012**, *26*, 490−496.
(81) Dalas, F.; Pourchet, S.; Nonat, A.; Rinaldi, D.; Sabio, S.; Mosquet, M. Fluidizing efficiency of comb-like superplasticizers: The effect of the anionic function, the side chain length and the grafting degree. *Cem. Concr. Res.* **2015**, *71*, 115−123.
(82) Uchikawa, H.; Hanehara, S.; Sawaki, D. The role of steric repulsive force in the dispersion of cement particles in fresh paste prepared with organic admixture. *Cem. Concr. Res.* **1997**, *27*, 37−50.
(83) Puthipad, N.; Ouchi, M.; Rath, S.; Attachaiyawuth, A. Enhanced entrainment of fine air bubbles in self-compacting concrete with high volume of fly ash using defoaming agent for improved entrained air stability and higher aggregate content. *Constr. Build. Mater.* **2017**, *144*, 1−12.

https://doi.org/10.1021/acs.langmuir.4c00762
Langmuir XXXX, XXX, XXX−XXX

(84) Xie, J.; Cui, X.; Guo, N.; Liu, G. Influence of Mix Proportions on Rheological Properties, Air Content of Wet Shotcrete—A Case Study. *Appl. Sci.* **2021**, *11*, No. 3550.
(85) Mousavinezhad, S.; Gonzales, G. J.; Toledo, W. K.; Garcia, J. M.; Newtson, C. M. In *Mechanical Properties of Ultra-High-Performance Concrete Containing Natural Pozzolan and Metakaolin*, Tran-SET 2022, 2022.
(86) Brennan, M. J.; Hollingshead, S. E.; Wilker, J. J.; Liu, J. C. Critical factors for the bulk adhesion of engineered elastomeric proteins. *R. Soc. Open Sci.* **2018**, *5*, No. 171225.
(87) Powers, T. C.; Willis, T. F. *The Air Requirement of Frost resistant Concrete*; Highway Research Board, 1950; Vol. *29*.
(88) Richardson, M.Degradation of Concrete in Cold Weather Conditions. *Durability of Concrete and Cement Composites*; Elsevier, 2007; pp 282−315.
(89) Micro Photonics. *Structural Parameters Measured by Skyscan™ CT-Analyzer Software*, n.d.
(90) Bažant, Z. P.; Chern, J.-C.; Rosenberg, A. M.; Gaidis, J. M. Mathematical Model for Freeze-Thaw Durability of Concrete. *J. Am. Ceram. Soc.* **1988**, *71*, 776−783.
(91) Liu, Q.; Chen, Z.; Yang, Y. Effect of fly ash on the air void size distribution entrained by selected anionic, cationic and nonionic surfactants in hardened cement mortars. *Cem. Concr. Compos.* **2021**, *124*, No. 104253.
(92) Qiao, M.; Chen, J.; Yu, C.; Wu, S.; Gao, N.; Ran, Q. Gemini surfactants as novel air entraining agents for concrete. *Cem. Concr. Res.* **2017**, *100*, 40−46.
(93) Zhang, X.; Zhang, H.; Gao, H.; He, Y.; Jiang, M. Effect of bubble feature parameters on rheological properties of fresh concrete. *Constr. Build. Mater.* **2019**, *196*, 245−255.
(94) Powers, T. *The Properties of Fresh Concrete*; John Wiley & Sons: New York, 1968.
(95) Bell, M. S.; Borhan, A. A Volume-Corrected Wenzel Model. *ACS Omega* **2020**, *5*, 8875−8884.
(96) Al-Kheetan, M. J.; Rahman, M. M.; Chamberlain, D. A. Moisture evaluation of concrete pavement treated with hydrophobic surface impregnants. *Int. J. Pavement Eng.* **2020**, *21*, 1746−1754.
(97) Karthick, S.; Park, D. J.; Lee, Y. S.; Saraswathy, V.; Lee, H. S.; Jang, H. O.; Choi, H. J. Development of water-repellent cement mortar using silane enriched with nanomaterials. *Prog. Org. Coat.* **2018**, *125*, 48−60.
(98) Huo, J.; Wang, Z.; Guo, H.; Wei, Y. Hydrophobicity Improvement of Cement-Based Materials Incorporated with Ionic Paraffin Emulsions (IPEs). *Materials* **2020**, *13*, No. 3230.
(99) Mora, E.; González, G.; Romero, P.; Castellón, E. Control of water absorption in concrete materials by modification with hybrid hydrophobic silica particles. *Constr. Build. Mater.* **2019**, *221*, 210−218.
(100) Qiu, Y.; Zhang, L.; Chen, Y.; Liu, Y.; Zhang, F. Experimental Study on Application Performance of Foamed Concrete Prepared Based on a New Composite Foaming Agent. *Adv. Mater. Sci. Eng.* **2022**, *2022*, No. 7217479.
(101) Kozłowski, M.; Kadela, M. Mechanical Characterization of Lightweight Foamed Concrete. *Adv. Mater. Sci. Eng.* **2018**, *2018*, No. 6801258.
(102) Hashim, M.; Tantray, M. Comparative study on the performance of protein and synthetic-based foaming agents used in foamed concrete. *Case Stud. Constr. Mater.* **2021**, *14*, No. e00524.
(103) Falliano, D.; De Domenico, D.; Ricciardi, G.; Gugliandolo, E. Experimental investigation on the compressive strength of foamed concrete: Effect of curing conditions, cement type, foaming agent and dry density. *Constr. Build. Mater.* **2018**, *165*, 735−749.
(104) Mendes, J. C.; Moro, T. K.; Figueiredo, A. S.; Silva, K. D. d. C.; Silva, G. C.; Silva, G. J. B.; Peixoto, R. A. F. Mechanical, rheological and morphological analysis of cement-based composites with a new LAS-based air entraining agent. *Constr. Build. Mater.* **2017**, *145*, 648−661.
(105) Sheng, Y.; Lin, K.; Binks, B. P.; Ngai, T. Ultra-stable aqueous foams induced by interfacial co-assembly of highly hydrophobic particles and hydrophilic polymer. *J. Colloid Interface Sci.* **2020**, *579*, 628−636.
(106) Binks, B. P.; Horozov, T. S.Colloidal Particles at Liquid Interfaces: An Introduction. *Colloidal Particles at Liquid Interfaces*; Cambridge University Press, 2006; pp 1−74.
(107) Hunter, T. N.; Pugh, R. J.; Franks, G. V.; Jameson, G. J. The role of particles in stabilising foams and emulsions. *Adv. Colloid Interface Sci.* **2008**, *137*, 57−81.

https://doi.org/10.1021/acs.langmuir.4c00762
Langmuir XXXX, XXX, XXX−XXX